NASA/CR-2008-215315

Pressure and Thrust Measurements of a High-Frequency Pulsed-Detonation Actuator

Namtran C. Nguyen and Andrew D. Cutler
The George Washington University, Newport News, Virginia

June 2008

The NASA STI Program Office . . . in Profile

Since its founding, NASA has been dedicated to the advancement of aeronautics and space science. The NASA Scientific and Technical Information (STI) Program Office plays a key part in helping NASA maintain this important role.

The NASA STI Program Office is operated by Langley Research Center, the lead center for NASA's scientific and technical information. The NASA STI Program Office provides access to the NASA STI Database, the largest collection of aeronautical and space science STI in the world. The Program Office is also NASA's institutional mechanism for disseminating the results of its research and development activities. These results are published by NASA in the NASA STI Report Series, which includes the following report types:

- TECHNICAL PUBLICATION. Reports of completed research or a major significant phase of research that present the results of NASA programs and include extensive data or theoretical analysis. Includes compilations of significant scientific and technical data and information deemed to be of continuing reference value. NASA counterpart of peer-reviewed formal professional papers, but having less stringent limitations on manuscript length and extent of graphic presentations.

- TECHNICAL MEMORANDUM. Scientific and technical findings that are preliminary or of specialized interest, e.g., quick release reports, working papers, and bibliographies that contain minimal annotation. Does not contain extensive analysis.

- CONTRACTOR REPORT. Scientific and technical findings by NASA-sponsored contractors and grantees.

- CONFERENCE PUBLICATION. Collected papers from scientific and technical conferences, symposia, seminars, or other meetings sponsored or co-sponsored by NASA.

- SPECIAL PUBLICATION. Scientific, technical, or historical information from NASA programs, projects, and missions, often concerned with subjects having substantial public interest.

- TECHNICAL TRANSLATION. English-language translations of foreign scientific and technical material pertinent to NASA's mission.

Specialized services that complement the STI Program Office's diverse offerings include creating custom thesauri, building customized databases, organizing and publishing research results ... even providing videos.

For more information about the NASA STI Program Office, see the following:

- Access the NASA STI Program Home Page at ***http://www.sti.nasa.gov***

- E-mail your question via the Internet to help@sti.nasa.gov

- Fax your question to the NASA STI Help Desk at (301) 621-0134

- Phone the NASA STI Help Desk at (301) 621-0390

- Write to:
  NASA STI Help Desk
  NASA Center for AeroSpace Information
  7115 Standard Drive
  Hanover, MD 21076-1320

NASA/CR-2008-215315

Pressure and Thrust Measurements of a High-Frequency Pulsed-Detonation Actuator

Namtran C. Nguyen and Andrew D. Cutler
The George Washington University, Newport News, Virginia

National Aeronautics and
Space Administration

Langley Research Center
Hampton, Virginia 23681-2199

Prepared for Langley Research Center
under Cooperative Agreement NNL06AA16A

June 2008

Available from:

NASA Center for AeroSpace Information (CASI)
7115 Standard Drive
Hanover, MD 21076-1320
(301) 621-0390

National Technical Information Service (NTIS)
5285 Port Royal Road
Springfield, VA 22161-2171
(703) 605-6000

Abstract

This paper describes the development of a small-scale, high-frequency pulsed detonation actuator. The device utilized a fuel mixture of H_2 and air, which was injected into the device at frequencies of up to 1200 Hz. Pulsed detonations were demonstrated in an 8-inch long combustion volume, at ~600 Hz, for the $\lambda/4$ mode. The primary objective of this experiment was to measure the generated thrust. A mean value of thrust was measured up to 6.0 lb, corresponding to specific impulse of 2611 s. This value is comparable to other H_2-fueled pulsed detonation engines (PDEs) experiments. The injection and detonation frequency for this new experimental case was ~600 Hz, and was much higher than typical PDEs, where frequencies are usually less than 100 Hz. The compact size of the model and high frequency of detonation yields a thrust-per-unit-volume of approximately 2.0 lb/in^3, and compares favorably with other experiments, which typically have thrust-per-unit-volume values of approximately 0.01 lb/in^3. This much higher volumetric efficiency results in a potentially much more practical device than the typical PDE, for a wide range of potential applications, such as high-speed flow boundary layer separation control, for example in hypersonic engine inlets, and propulsion for small aircraft and missiles.

Table of Contents

List of Figures

List of Tables

Chapter 1 - Introduction

Section 1.1 Motivation

It has long been a goal of research within the field of propulsion to design low cost systems that will perform well at varying flight conditions and still maintain reasonable efficiencies. This goal applies not only to engines designed for airplanes (commercial or military) but also to space vehicles and small-scale propulsion applications. Numerous studies have been conducted with pulsed-combustion, which shows promise as an efficient propulsive device. In recent years, research has shown that the pulse detonation engine may be a useful alternative to traditional methods of propulsion. The appeal of the pulse detonation engine is that it has the potential to produce high specific impulse. Another advantage is that it does not have many complex moving parts; therefore, it potentially is much simpler and less expensive to produce.

Various applications have been considered and researched for pulse detonation engines. These range from propulsive applications in small aircraft and missiles to pressure-rise combustors for gas turbine engines [1], or high-speed flow control devices for boundary layer separation control [2].

Section 1.2 Background

Pulse Detonation Engines, or PDEs, are unsteady propulsion devices that use repetitive detonations to produce a periodic impulse [3]. The PDE differs from conventional propulsion systems in that it relies on detonation rather than deflagration of the fuel/air mixture to produce thrust. The detonation wave speed is approximately two orders of magnitude higher than that of a typical deflagration wave [3]; namely, ~6750 ft/s for an ideal detonation in a stoichiometric hydrogen/air mixture. As defined by Chapman and Jouget, around 1900, the detonation wave was defined to be a shock wave followed by combustion [4]. Consequently, the velocity at which the detonation wave travels down the combustion chamber is known as the Chapman-Jouget (C-J) velocity if the combustion occurs at a Mach number equal to one.

The C-J velocity is an ideal detonation wave speed pertaining to the speed in a long, constant area tube filled with reactants. On the other hand, deflagration is defined as the subsonic combustion of reactants propagating through a process of diffusion, possibly enhanced by turbulence. A PDE is an engine cycle in which a tube is periodically filled with reactants and a detonation is initiated in it. Early theoretical analysis of pulsed detonation systems have indicated that very high specific thrusts can be attained from the use of PDEs [5].

An ideal PDE cycle can be broken into four phases: (1) initiation of the detonation wave; (2) propagation of the detonation wave; (3) exhaust of combustion products; and (4) refilling of reactants [3]. First, the combustion volume is filled with a combustible fuel/air mixture. Ignition of the mixture occurs at the closed end of the combustion chamber, and detonation is initiated. The resulting detonation wave travels down to the open end of the tube. When the detonation wave reaches the open end, the strong compression wave is reflected as an expansion wave. The expansion wave travels to the closed end, causing the

products of the combustion to be purged from the volume. A new charge of the combustible fuel/air mixture fills the volume, and the cycle starts again. Experiments with PDEs typically operate in a quasi-steady state manner in which hot combustion products are purged relatively slowly from the combustion volume, by displacing with air, before filling (again relatively slowly) with a new charge of reactants.

Figure 1 shows a schematic of a typical experimental PDE cycle [6]. First, combustion products from the previous cycle are purged from the tube using air (Step 1). Then, the detonation tube is filled with a reactant fuel mixture (Step 2). The reactants are ignited by an ignition source located at the end of the detonation tube (Step 3). Shock waves, formed from combustion of reactants, coalesce and cause deflagration-to-detonation (DDT) transition (Step 4). After the detonation wave exits the tube, an expansion fan propagates toward the open end of the detonation tube (Step 5). Pressure within the detonation tube is reduced to static, atmospheric conditions. For the PDE cycle shown in Figure 1, the cycle is complete when the detonation tube is at ambient conditions and the flow within the tube is stationary (Step 6) [6].

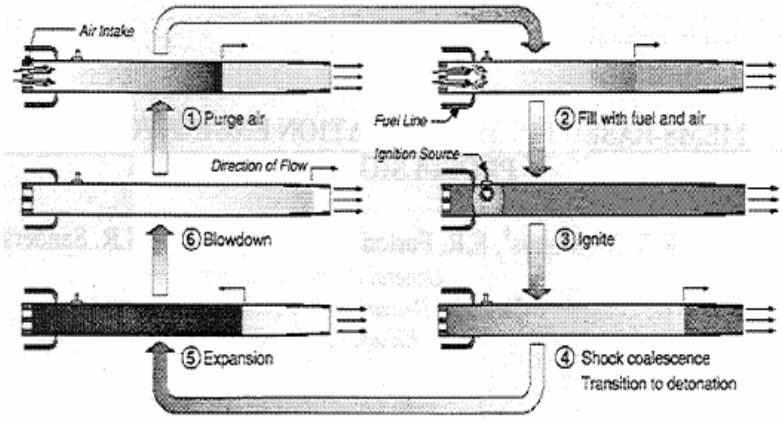

Figure 1: Experimental pulse detonation engine cycle, from McManus *et al.* [6].

In recent years, studies have been conducted involving active boundary layer control techniques using pulsed combustion [7]. These techniques work by manipulating the unstable free shear layer, thus exploiting the Coanda-like effect for unsteady reattachment [7]. In high-speed boundary layer control applications, pulsed or synthetic jets require both high impulse and high frequency in order to be effective [2]. Combustion-driven fluidic actuation has the potential to yield a high momentum jet by exploiting the chemical energy of the reactant fuel/air mixture [7]. Because of its potential to yield high impulse and the ability to operate at high frequencies, the PDE has potential as an effective flow control device.

1.2.1 Historical Background

Pulsed combustion was first identified as a self-sustaining process by David L. Chapman and Jacques C.E. Jouget around 1900 [6]. The first reported work with cyclic pulsed combustion is attributed to N. Hoffman in 1940 [4]. Hoffman's experiments employed acetylene-oxygen and benzene-oxygen fuel mixtures to create intermittent detonations in a long, narrow tube [4]. In his studies, Hoffman could achieve intermittent detonations in only

a narrow range of ignition frequencies. Hoffman attempted to experimentally find the optimum injection frequency, but further work was halted because of the onset of World War II [4].

The first full-scale application of pulsed propulsion was the V-1 "flying buzz bomb", developed by the German Luftwaffe, German Air Force, during WWII 46 [8]. The V-1 was a small missile powered by an Argus As 014 pulse jet engine that operated at 50 cycles per second, which gave the V-1 its characteristic sound [8]. One drawback to the V-1 was that it could not operate at speeds below 150 mph. Thus, it required a boosted launch provided by a catapult, which accelerated the V-1 up a 180-foot ramp to a launch speed of 200 mph [8]. The propulsion system used in the V-1 is an example of a pulsejet, not a pulse-detonation engine. The distinction is that in a pulsejet, combustion is by deflagration in a tube resonating in the quarter-wave mode; detonations do not occur, and consequently, the amplitude of pressure fluctuations in the engine is much less.

Work on intermittent detonations picked up after the end of the war with a team led by J.A. Nicholls. Experiments conducted under Nicholls focused on the use of intermittent detonation waves as a means of thrust [9]. In these experiments, a detonation tube was suspended using wires so that thrust would cause the model to swing like a pendulum. Four reactant mixtures were tested: H_2/O_2, H_2/air, acetylene/O_2, and acetylene/air. Variation of thrust with time was measured using an accelerometer mounted to the center of the detonation tube [5]. When the mixture ratio was adjusted correctly, sharp, clear, and even explosions were observed at frequencies up to 35 Hz [5]. In the end, Nicholls and his team concluded that the intermittent detonation engine had many advantages, including its mechanical simplicity, static thrust capabilities, efficient operation at supersonic velocities, and potential high thrust levels or high fuel economy, but no useful applications were pursued[5].

1.2.2 PDE vs. Pulsejet Engine

The PDE and the pulsejet engine are similar in that they are both unsteady gas generators which are combustion driven, and the combustion which takes place is approximated as a constant-volume heat release process, though only marginally in the case of the pulsejet [10]. However, a fundamental difference between the PDE and the pulsejet engine is the method of combustion. In a pulsejet, combustion is confined to deflagration only; therefore there is no phase of initiation and propagation of the detonation wave, as with the PDE. Also, during the pulsejet operation cycle, heat is released both before and after the minimum specific volume, or maximum pressure, is reached, which makes the pulsejet engine less efficient as a thrust-producing device [10]. However, studies have shown that the pulsejet engine may be competitive in terms of its static performance, though still not as promising as the PDE [10].

Another difference between the PDE and the pulsejet is that the pulsejet incorporates a tube in which a quarter-wave resonance is established. The combustion volume is at the closed end of the tube, where the amplitude of the pressure fluctuations is highest, and injection and combustion of reactants is timed so as to reinforce the existing pressure fluctuations. As previously mentioned, existing practical PDEs operate in a quasi-static manner, rather than in resonance.

A comparison between the performance of the pulsejet engine and the PDE was

conducted using a Solar PJ32, which is a 1/5-scale model of the Argus V-1 pulsejet engine developed for the Navy in 1951 [10], operating on 100 Octane, low-lead Aviation Grade Gasoline. Pulsejet performance results were compared to data collected previously from a statically operated PDE of similar length scales, run at stoichiometric conditions [10]. Measured thrust peaked at 102 lb at the upper limit of 4.5 lb_m/min fuel flow, corresponding to specific impulse ranging between 1400-1500 s [10]. This is comparable to previously measured PDE results at similar conditions, which would yield a specific impulse around 1800 s. However, the fill fraction of the pulsejet was very low, and PDE performance is hypothesized to increase dramatically, I_{sp} = 6000-8000 s, as the fill fraction of the PDE is reduced to that of the pulsejet [10].

1.2.3 Work with Hydrogen-Fueled PDEs and Pulsejet Engines

Several studies have been conducted for PDEs and pulsejet engines using H_2/air fuel mixtures. Investigations conducted at the General Electric Global Research Center have used ejectors to augment the thrust generated by a 2" ID x 36" PDE tube burning a stoichiometric hydrogen-air fuel mixture at a frequency of 10 Hz [11]. In these experiments, the PDE tube was mounted to a thrust stand, which included a mass-spring-damper system with a thrust sled mounted on low friction bearing [11]. Movement of the thrust stand was measured using a load cell. The ejectors tested were mounted to a straight rail and connected to a stepping motor, so that the ejectors could be translated relative to the PDE tube. General results show that the PDE generated a thrust of 12.9 lb, which was augmented 14% by the presence of an ejector [11].

A separate study of a H_2-fueled high-frequency pulse detonation engine tested a much longer PDE tube geometry, 2.952" ID x 86.614" long [12]. Successful tests were achieved at a maximum operating frequency of 32 Hz. In these experiments, the use of Shchelkin wire (SW) was used to study its effect on lengthening or shortening the DDT distance in the PDE tube [12]. Two SW lengths were studied, 600 mm and 1400 mm, and yielded maximum specific impulse of 1800 s and 2380 s, respectively [12].

Detonation studies were also conducted at the Air Force Research Laboratory using aluminum tubes, 2" ID and 36" in length [13]. Although the PDE developed at AFRL has a broad operating range and configuration options, with the capability of four detonation tubes operating side-by-side at up to 100 Hz each, the experiment only used a single aluminum tube operating at 16 Hz[13]. Pulsed thrust measurements were taken using a damped thrust stand mounted to an existing large capacity static thrust stand [13]. Results show that thrust increased linearly with injection frequency, i.e. in proportion with fuel flow rate, at approximately 0.46 lb/Hz, using stoichiometric pre-mixed H_2/air with a clean air purge fill ratio of 50% [13]. Cold, clean air was used as a purge gas in these tests in order to prevent hot products from igniting the incoming charge of reactants and to partially cool the inside of the detonation tube. In tests with a fill fraction of 1.0, generated thrust measured approximately 5.0 lb, and specific impulse was calculated to be approximately 3750 s [13]. Investigators concluded that PDE performance results are highly scalable to different injection frequencies and tube geometries.

Another study conducted at AFRL was aimed at developing an enhanced combustion pulsejet engine (ECPE) for applications at Mach 0 to Mach 3 [6]. Single shot detonation and cyclic detonation, operation at 100 Hz, pulsejet tube experiments were carried out using a

variety of fuel-air mixtures, including H_2/O_2, H_2/air, ethylene/air, and ethylene/O_2 [6]. Thrust measurements were not taken for these experiments, but results support the hypothesis that combustion enhancement in pulsejet engines may lead to improvements in pulsejet performance [6].

1.2.4 Thermodynamic Cycle Analysis and Performance Prediction

Classical, closed thermodynamic cycle analysis of the fundamental PDE has been compared to ideal and real cycle analyses of the Brayton and Humphrey cycles [14]. Results show that the efficiency of the PDE cycle is comparable to the Humphrey cycle, which is more efficient than the Brayton cycle typically used to predict the performance of most propulsion systems [14]. The thermodynamic efficiencies for the three cycles were found to be 27% for the constant-pressure Brayton cycle, 47% for the constant-volume Humphrey cycle, and 49% for the detonation cycle [9]. In all three cases, the amount of heat addition was kept the same, and the reactant mixtures were compressed adiabatically from 1 atm to 3 atm before heat addition occurred. Products of combustion were expanded adiabatically to 1 atm, and then the system was returned to its initial state [9]. The use of detonations as a means of propulsion may lead to more compact and efficient systems because of its performance is comparable to the constant volume cycle.

An analytical study of the propulsive performance of a H_2-fueled single tube PDE with the convergent-divergent nozzle yielded a cycle-averaged specific thrust of 862 m/s^2 and specific impulse of 3402 s, which is 46% higher than that achieved with a straight tube [3]. Further analysis showed that the CD nozzle significantly improved the engine performance by helping preserve the chamber pressure rather than by producing significant thrust. It was also found that specific impulse decreased by 6.5% as the refilling Mach number increased from 0 to 0.93 [3]. It was unclear whether this performance loss is directly related to the refilling Mach number.

A study of the effect of nozzle configuration on propulsive performance found that the nozzle length for nominal perfect-expansion should be 20-25% of the overall length of the PDE [3]. Results showed that nozzle length played a minor role in determining the PDE performance, with a decrease in specific impulse of 1%. It was found that small nozzle throat diameter (25% smaller than the baseline configuration) resulted in a 5.6% increase in specific impulse to 3597 s; however, exceedingly small diameter nozzle throats may cause internal flow losses due to the increase in the presence of shock waves from severe geometric constraints [3]. Further studies of the thrust chamber dynamics in a single-tube air-breathing PDE must consider multi-cycle operations to generate more relevant results.

Section 1.3 Objectives

1.3.1 Previous Work at NASA Langley Research Center

Research at the NASA Langley Research Center has been conducted toward the development of a pulsed detonation actuator for high-speed flow control [2][15]. This work originated in support of NASA's Flow Control Program; it was motivated by the need for pulsed jet flow control actuators with greater control authority than existing pulsed and synthetic – i.e., zero net mass flux – jet actuators. The first generation model had a combustion volume with a rectangular cross section of 1.52" x 1.19" near the bottom, which

transitions to a circular cross section 1.52” in diameter between x=6” and x=8” (reference x=0” at the base of the combustion volume). The combustion tube was tested at various lengths using cylindrical extension tubes of constant area. The typical testing length was 16”. In some cases, the cylindrical section of the combustion volume was closed with a circular nozzle, which has a 0.625” throat diameter, and in others the nozzle was removed to allow the combustible mixture to discharge directly into the laboratory atmosphere. Windows located along the length of the rectangular section of the combustion volume (x=0” to x=6”) allowed for flow visualization within the device. An additional window at the bottom of the device allowed a laser light sheet to pass through the plane of symmetry of the combustion volume.

The high-speed valve assembly is driven by a motor, which is in turn controlled by the data acquisition program. The valve is composed of a rotating shaft, shown in Figure 2, supported by high-speed bearings. The shaft rotates in a close-fitted housing with passages for air and H_2 [2][15]. H_2 and air pass through the valve through a hole and a slot, respectively. The reactants are combined in a small nozzle before entering the combustion volume at x=1.15”. The shaft is turned by a high-speed motor, capable of up to ~45,000 rpm. An automobile sparkplug is located directly opposite the reactant injection and is continuously fired at 120Hz, independent of the injection frequency.

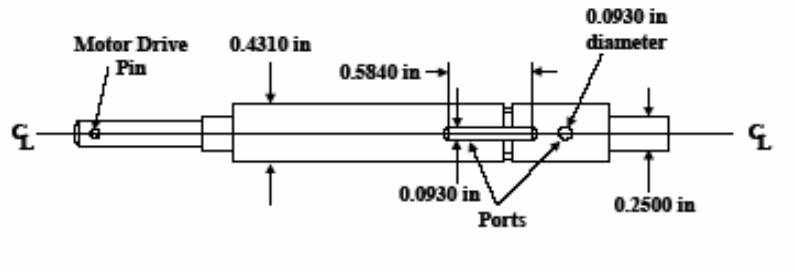

Figure 2: Detail of rotating shaft, from Cutler *et al.,* 2005-06[2][15].

For the first generation actuator model, six reactant flow rates were studied: three without combustion (air-only) and three with near-stoichiometric proportions of H_2 and air. General results show that pressure fluctuations were strongest and most ordered at resonant conditions [15]. The resonant frequency was determined by the length of the tube and could be raised by shortening the tube. It was observed that the highest pressure fluctuation levels were attained when the length of the tube filled with reactants was the largest; this also resulted in periodic detonation-like behavior of the combustible mixture. As the combustion tube length was reduced to raise the frequency of resonance, the maximum length of tube that could be filled by reactants in one cycle by the existing valve was reduced, and detonations were not observed. It was speculated from these results that periodic detonations could be achieved with the existing valve at higher frequency if the cross-sectional area of the volume was decreased, with flow rates kept the same and length decreased to raise the frequency for a particular mode.

A second generation actuator model was developed to test the hypothesis that detonations would be present at higher frequencies if a sufficiently large length of the tube was filled with the reactant mixture. Many configurations were tested before the final second generation model design was chosen. Various combustion tube lengths, injection points, and

injection directions were tested to determine which configuration would yield the most organized, periodic detonations.

This model was designed to be modular, with tube sections that could be screwed into one another to provide different lengths of the combustion volume, and different orientations and locations of reactant injection. Unlike the previous model which transitioned from a rectangular cross-section at the ignition area to a circular cross-section toward the exit, the combustor tube is circular throughout, with a constant inner diameter of 0.75". The model did not contain any windows. An identical high-speed valve and motor assembly were used as in the previous model. Experiments were conducted to determine the optimum location and direction for injection of the reactant mixture, and reactant mixture injection into the combustion volume through a square nozzle (0.335" x 0.335") located 4.5" from the bottom, at a downward angle of 30° was found to produce the best results. Results reported were for a combustion tube length of 8" [2].

Data were collected for 8 cases: two with air only (no combustion) and six with a stoichiometric mixture of H_2/air. Periodic detonations were observed in the $\lambda/4$ resonant frequency mode with an injection frequency of approximately 600 Hz, and periodic deflagrations were observed in the $3\lambda/4$ resonant frequency mode with an injection frequency of approximately 1400 Hz [2]. For the $\lambda/4$ resonant frequency mode, RMS pressure was found to be greatest at the closed end of the detonation tube and lowest near the exit. Results show that if fill fraction is approximately 1 (i.e. the tube is completely filled with reactants), then the peak pressure rise approaches approximately 80% of the C-J detonation pressure rise [2]. It is believed that detonations were initiated in these experiments by the trapped products from the previous cycle at the closed end of the combustion tube [2]. Indeed, at many operating conditions, pulsed detonation combustion was self-sustained without use of the spark.

1.3.2 Current Work

The present project is an extension of the work done by Cutler, *et al*., in which pulsed combustion of near-stoichiometric H_2/air fuel was observed in chambers of varying size and geometry at various injection frequencies [2][15]. As in the previous experiments, measurements of pressure at various locations in the combustion volume, pressure, temperature and rate of flow of the reactants, and injection frequency were collected. The major difference between the present test and previous tests is that thrust and I_{sp} generated by the model is also measured.

In previous work, results showed that the developed pulsed detonation actuator had the potential of performing well in flow control or propulsive applications [7]. In order for a small-scale, high-frequency pulsed-detonation device to be considered for these applications, it must be demonstrated that it provides significant thrust. Thus, the main contribution of the present work is the measurement of thrust and I_{sp}. The current work was developed and tests were conducted to determine the thrust and I_{sp} generated by the model. A thrust balance was set-up in the laboratory to measure the thrust generated, and specific impulse was calculated. Comparisons were made between the device discussed here and other hydrogen-fueled pulsed detonation experiments researched at other facilities.

This paper provides detailed documentation of the experiment. A description of the new model and the thrust balance set-up, as well as the data acquisition system and other

instruments used, is presented in Chapter 2. Experimental procedures, test conditions, and method of data reduction are explained in Chapter 3. Results are presented and discussed in Chapter 4, and compared to other experiments using H_2-fueled pulsed detonation devices. Also, future work in this field and possible applications based on the present results are considered.

Chapter 2 - Test Hardware and Equipment

Section 2.1 Actuator Model and High-Speed Valve

Modifications to the second generation actuator model, developed by Cutler *et al*. [2], led to the development of a third generation actuator model, which is discussed in the present paper. As opposed to the previous model, the cross-sectional area of this model was reduced, while maintaining the same length, and the valve shaft hole areas were increased to allow delivery of a greater flow rate of reactants, both changes leading to a greater reactant fill fraction. Also, rather than a circular cross-section, this model had a rectangular cross-section to allow installation of windows and future visualization of the internal flow. (No visualization of the flow was performed in the present work.) Figure 3 is a rendering of the model and a photograph of the mounted assembly.

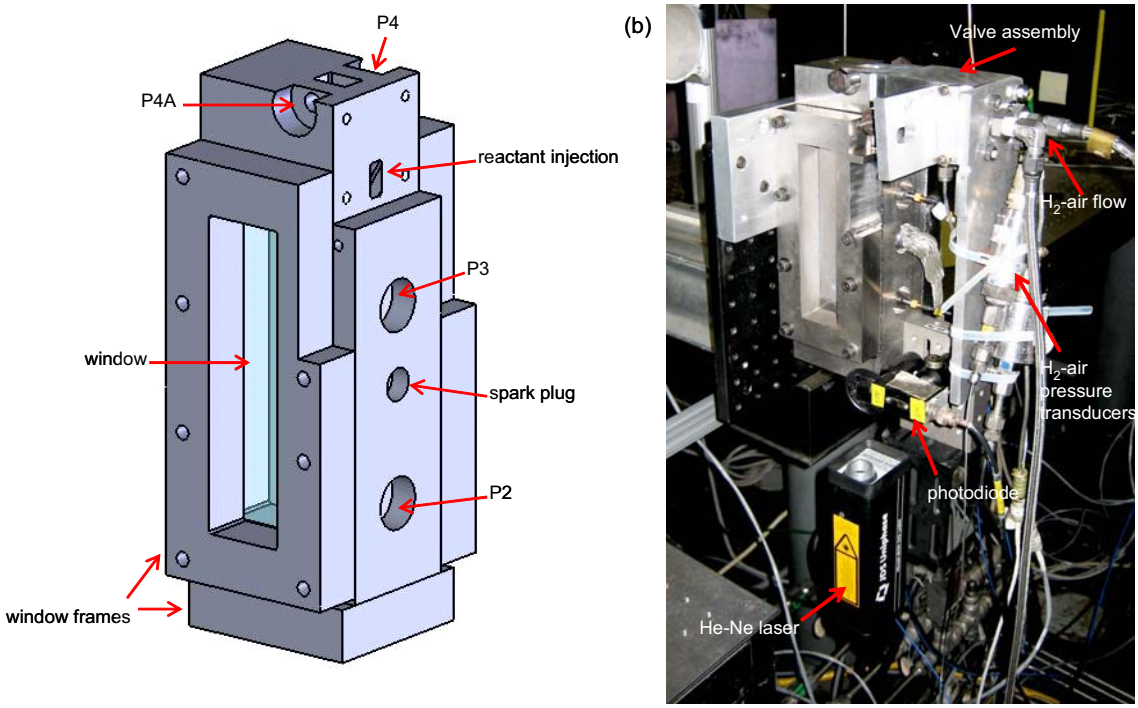

Figure 3: Third generation actuator model - (a) Computer rendering of model; (b) Photograph of mounted actuator assembly.

The combustion volume is 8” in length and has a constant rectangular cross section of 0.5” x 0.75”. As in the first generation model, windows located along the length of the combustion volume from the base of the combustion volume (x=0”) to x=6” allow for flow visualization within the device, and an additional window is provided at the bottom of the model to allow a laser light sheet to pass through the plane of symmetry. In the present work, these windows were replaced with stainless steel plates, and flow visualization was not conducted. A reactant mixture is injected into the combustion volume at a downward angle of 30° at x=5.75” through a 0.335” × 0.335” square nozzle. An automobile sparkplug is located at x=2.75” and is fired continuously at 120 Hz, independent of the injection frequency. Pressure taps P2, P3, P4, and P4A are located at x=0.25”, 4.25”, and 7.75”, respectively. There is no pressure tap at P1 – this numbering nomenclature is used for consistency with data acquisition channels, discussed in Section 2.3.

The design of the model is very massive to provide a heat sink. The model is not actively cooled so making it massive allows for the model to be operated longer before it heats up beyond a specified limit. Excessive rise in temperature would damage the high-frequency pressure gauges. Warping of the model due to non-uniform heating would lead to breaking of the windows. Warping of the high-speed valve assembly due to non-uniform heating would cause binding of the shaft and failure of the bearings.

The high-speed valve and motor assembly used in the previous studies was modified for the present device. Figure 4 is a computer rendering of the high-speed valve assembly and rotating shaft. The high-speed valve is composed of a rotating shaft, which is supported by high-speed bearings and contained in a close-fitting housing assembly. The rotating shaft is equipped with a hole and a slot to provide the H_2 and air, respectively. As shown in Figure 4, the hole and slot in this valve are slightly larger than in the previous models. The diameter/width of the ports was increased from 0.0930" to 0.140" to allow for easier passage of the gasses and reduce the load on the high-speed bearings. All other dimensions remained the same as in the shaft shown in Figure 2.

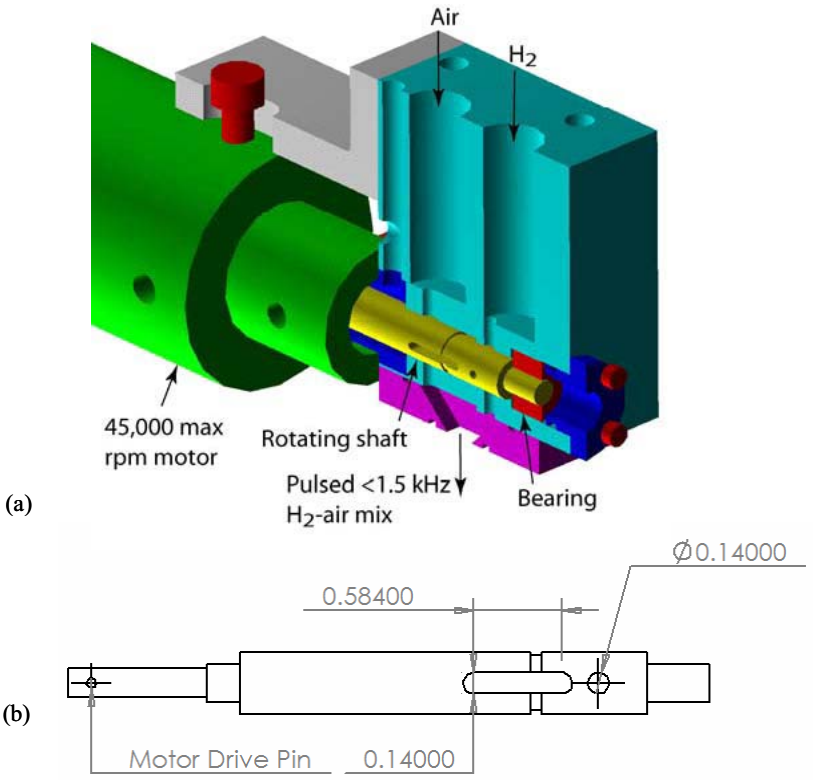

Figure 4: (a) Cut-away view of high-speed valve assembly, from Cutler *et al.*[2][15]; (b) Detail of rotating shaft, dimensions in inches.

The housing assembly for the rotating shaft has corresponding passages to the ports on the shaft. When the ports in the rotating shaft and the passages in the housing assembly align, twice per revolution, a mixture of H_2 and air passes through the valve into a small nozzle, where they are combined prior to being injected into the combustor. A DC drive motor (model CAT X360) turns the rotating shaft. The motor has a maximum speed of

45,000 rpm; it is controlled by a Minarik MC10-PCM adjustable DC motor controller[1], which can be set manually using the dial provided or remotely using a 0-10 VDC signal.

Section 2.2 Thrust Balance Set-up

(a)

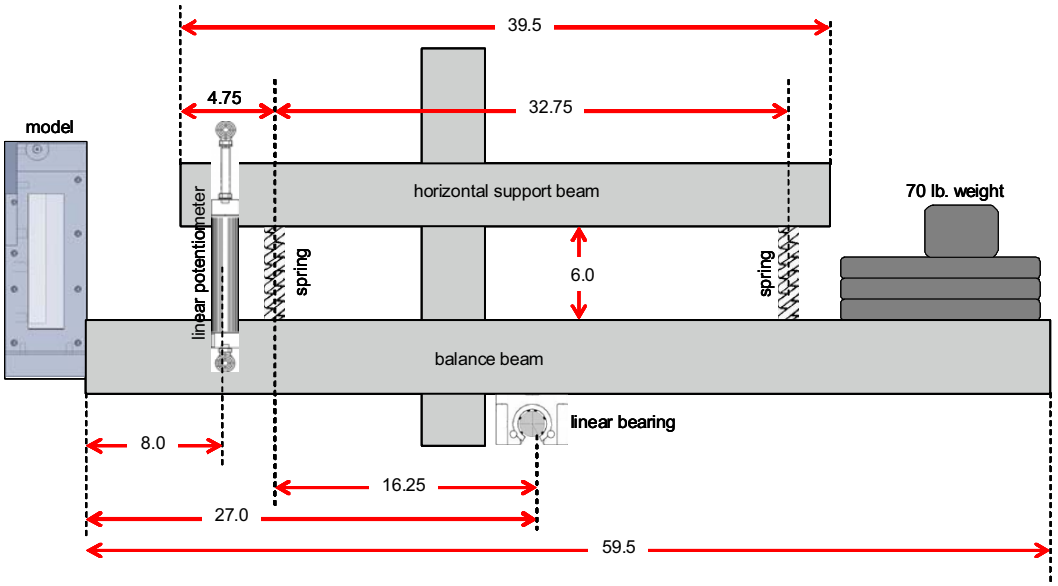

(b)

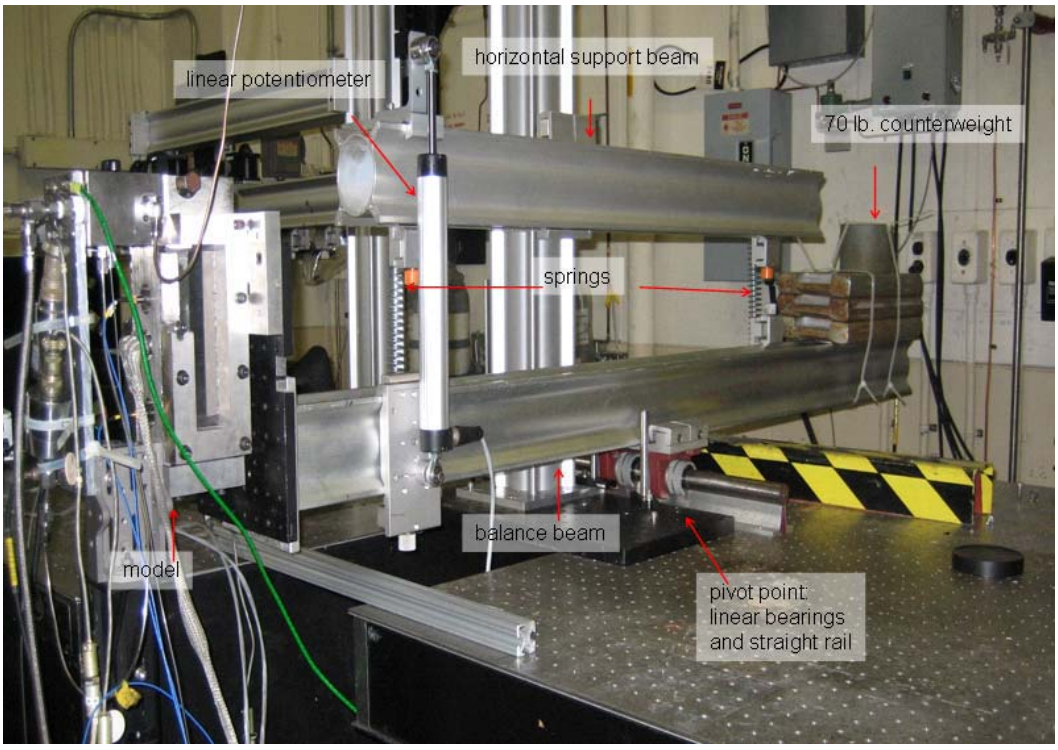

Figure 5: Simple sketch (a) and photograph (b) of thrust balance.

[1] Use of a trade name or trademark in this report is for accurate reporting and does not intend endorsement.

A thrust balance was designed in order to measure the thrust applied by the model. Several different configurations were attempted before settling on the final design. In the first design, the model was mounted vertically on a pair of rails using four linear ball bearings. The model then rested on a load cell, which would measure the force upon it. This method did not work because vibrations transmitted through the mechanism, which occurred during testing, were so strong that an accurate force measurement could not be made with the load cell.

To remedy this problem, the next design attempt replaced the load cell with four springs in compression, arranged in parallel, and a linear potentiometer. The model was still mounted vertically to a pair of rails; however, the motion of the model due to loads was much larger than in the previous attempt. Springs were used in order to damp out the vibrations caused by the model. A linear potentiometer was used to measure the model displacement, which was proportional to the force applied by the model. This set-up did not work because of friction and sticking of the linear bearings, caused in part by the considerable weight of the model (~70 lbs). In an attempt to reduce the load on the bearings, the model was suspended from above using a cable that was threaded through two pulleys and attached to heavy counter weights on the other end. However, rather than reducing the friction in the system, the pulley system introduced more friction.

The final design used a simple beam balance. Figure 5 is a simple sketch and photograph of the model and thrust balance used for this experiment. The actuator model is mounted to one end of an aluminum beam, while the other end is loaded with 70 lbs. to balance the weight of the model. The center of the beam is attached to a straight rail by means of a pair of linear ball bearings, which act as the fulcrum or pivot point for the system. Additionally, springs in tension are located on either side of the pivot point, connecting the beam to a horizontal support above, to provide a restoring force as the beam is deflected by thrust applied by the model.

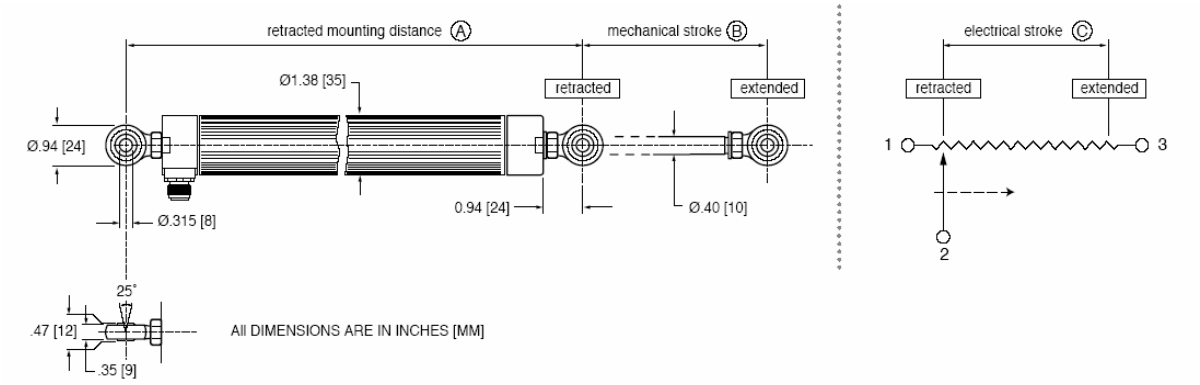

Figure 6: Outline drawing of CLWG-150-MC4 linear potentiometer, Celesco Transducer Products, Inc.

A linear potentiometer is attached to the system to measure displacement in response to thrust. Figure 6 is an outline drawing of the linear potentiometer. The retracted mounting distance (A) is 12.72", and the mechanical stroke (B) is 6.10". The electrical stroke (C) is 5.98". The sensor is made from a conductive plastic linear potentiometer and is housed in an aluminum enclosure. The linear potentiometer has a linearity of $\pm 0.08\%$. It has an input resistance of 5K ohms and can take a maximum input voltage of 25 V (AC or DC). The enclosed end of the linear potentiometer is mounted to the beam, and the extendable arm is

fixed to the horizontal beam support. Although the motion of the beam causes the linear potentiometer to pitch forward slightly, the angle of pitch is deemed negligible. The voltage across the potentiometer is read into the DAQ system when data are taken.

Section 2.3 Instrumentation and Experimental Procedure

Pressurized air, O_2, and gaseous H_2 fuel were supplied to the actuator through the valve, as stated previously. Flow of H_2 was measured using a 0-1000 standard liter per minute (SLPM) Hastings mass flow meter, and flow of air was measured using a 0-2500 SLPM Hastings mass flow meter manufactured by Teledyne Hastings Instruments. In runs where O_2-enriched air was used, flow of O_2 was measured using a 0-300 SLPM Hastings mass flow meter. The flow meters were connected to two Hastings Model 200 power supplies. Errors in flow meters are ~2%; random errors due to calibration are ±1-2%, whereas the flow meters read high ~1-2% per 100 psi above atmospheric pressure.

Pressure taps were provided in the valve to monitor the mean pressures of the supply H_2 and air. Valve shaft position was determined using a helium-neon laser aimed at the rotating shaft through the housing assembly of the motor. The laser light is reflected off a reflective spot on the shaft onto a photodiode once per revolution.

Time-resolved pressure measurements were taken within the combustion chamber at P2, P3, P4, and P4A, as indicated in Figure 3(a). These measurements were taken using 0-200 psi PCB-Piezotronics pressure sensor model 113A21. Figure 7 is a sketch of an installed pressure gauge. Pressure taps P2 and P3 have a diameter of 0.076", and two pressure taps of different size are located at the exit, P4 and P4A. The pressure tap on the right, P4, has a diameter of 0.076", whereas the one of the left, P4A, has a larger diameter of 0.109". Simultaneous pressure data were collected to compare the time response of these two pressure taps.

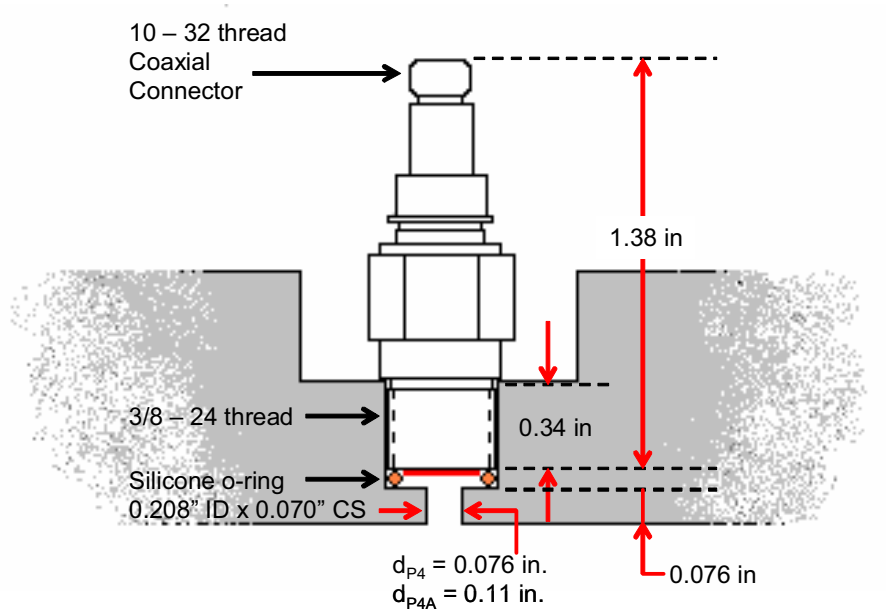

Figure 7: Sketch of installed pressure gauge.

Figure 8 is a simple schematic of the data acquisition system as it is set up in the

laboratory. On a typical run, during which data is collected for five seconds, a LabVIEW program that controls the experiment and acquires the data is initiated on the PC. An initial low motor speed is set manually using the motor controller. A/D trigger settings, scope channel settings, and voltage input settings are specified to the program. This data is then sent to a 4-channel LeCroy Waverunner LT-345 digital oscilloscope and a National Instruments SC-2345 signal conditioning unit, via a National Instruments PCI-6025E high-performance multipurpose I/O board contained in the PC. The specified initial voltage input value, which yields a low motor speed, is relayed from the SC-2345 through the motor controller to the motor.

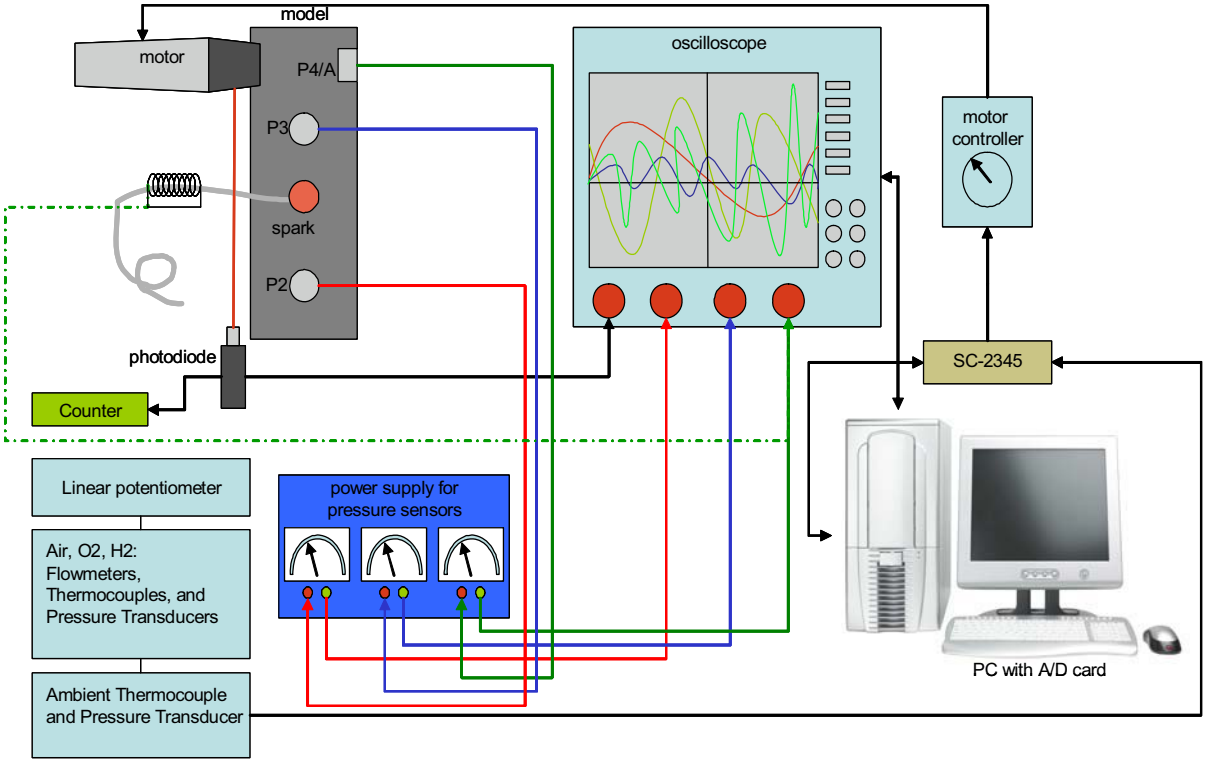

Figure 8: Simple schematic of data acquisition system.

Once specified reactant flow rates are established and combustion occurs, data acquisition is initiated through the LabVIEW program on the PC. The motor controller is switched from manual to signal, and the motor is ramped up to the specified final voltage input value, corresponding to high motor speed. The photodiode signal is displayed on Channel 1 of the oscilloscope, and the frequency of the motor is displayed on a counter. Pressure sensor data are also displayed on Channels 2-4 of the oscilloscope, through a 3-channel PCB-Piezotronics signal conditioning unit and power supply, model 480A21. Data are acquired at approximately 50,000 samples per second, per channel. Once data has been collected by the oscilloscope, i.e. after five seconds, it is downloaded to the PC.

Simultaneous H_2 and air flow rate, pressure, and temperature data, as well as the voltage reading from the linear potentiometer and ambient temperature and pressure, are also acquired using several analog I/O modules, manufactured by National Instruments, installed in the SC-2345. The pressure transducers used to measure H_2 flow, air flow and ambient

pressure were manufactured by MB Electronics. H_2 flow pressure was measured using pressure transducer model 151-BAA-1, with a range of 0-500 psi. Air flow pressure was measured using pressure transducer model PA830-300, with a range of 0-300 psi. Ambient pressure was measured using pressure transducer model 151-DBA-1, with a range of 0-25 psi. The thermocouples used to measure the temperatures of H_2 flow, air flow, and the laboratory atmosphere were manufactured by Omega Engineering, and each was connected to a cold junction compensator also manufactured by Omega Engineering. While data are being downloaded to the PC from the oscilloscope and through the SC-2345, the motor is returned to a low frequency, while any excess H_2 gas is purged from the laboratory area.

Several test runs were conducted which use a slightly different schematic than discussed above. When simultaneous pressure data of the two pressure tap locations at the exit (P4 and P4A) are taken, which will be discussed in Section 3.1, pressure data at P3 are not collected. Instead, P4A pressure data are collected and displayed on Channel 3 of the oscilloscope. During runs when steady-state thrust is to be measured, data are collected for ten seconds. Rather than specifying the voltage input to the SC-2345, a constant motor speed is attained by manually setting the motor controller. Pressure gauge data are not acquired for these tests to avoid damaging them. Tests were also conducted to investigate the role of the spark, which will be discussed in Section 4.3. During these tests, P4 pressure data were not collected. Instead, a voltage signal from a wire wrapped tightly around the spark plug wire was collected and displayed on Channel 4 of the oscilloscope.

Chapter 3 - Experimental Method and Data Reduction

Experiments were set-up and run in the CARS Laboratory, Room 204, located in the Hypersonic Airbreathing Propulsion Branch, Building 1221C, at the NASA Langley Research Center in Hampton, VA.

Section 3.1 Pressure Sensor and Force Balance Calibrations

Preliminary runs with air only at 1500 SLPM were conducted to validate the calibration coefficients for the pressure sensors used in subsequent test runs with and without combustion. The pressure sensors to be calibrated were installed into the P2 pressure tap, located at the bottom of the combustion volume. During a typical run, the valve motor was started at a low frequency as air flow rate was established. Data acquisition was initiated and the motor would scan a range of low to high frequencies. There were three new pressure sensors (S/N 16589, 16590, and 16591) for which manufacturer's calibration coefficients were available. The coefficients of the older sensors (S/N 8586, 8587, and 13386) were adjusted to match the response of the new gauges. Table 1 lists the adjusted calibration coefficients used for the various pressure sensors. Figure 9 is a plot of root-mean-square pressure fluctuation at P2 versus injection frequency for the six pressure sensors used, after adjusted calibration coefficients were applied.

Periodically throughout the testing period the calibration of the pressure sensors was checked, and the calibrations adjusted if required to accommodate any changes that may have occurred due to the extreme conditions to which the sensors were exposed (i.e. high heat, strong vibrations). Although calibration coefficients did change, the difference was small, no larger than 9.5% in extreme cases, but usually $\sim \pm 3\%$. Another problem that was encountered with the pressure sensors is that they would sometimes fail during testing. Often, the sensor in a given tap would need to be switched with a different sensor, and the case would have to be repeated. Sensor failure usually occurred at high reactant flow rates and was most likely caused by the extreme conditions present in the volume during combustion.

Sensor S/N	Calibration Coefficient [V/psi]
8586	0.02455
8587	0.02925
13386	0.02225
16589	0.02342
16590	0.02328
16591	0.02375

Table 1: Calibration coefficients for pressure sensors.

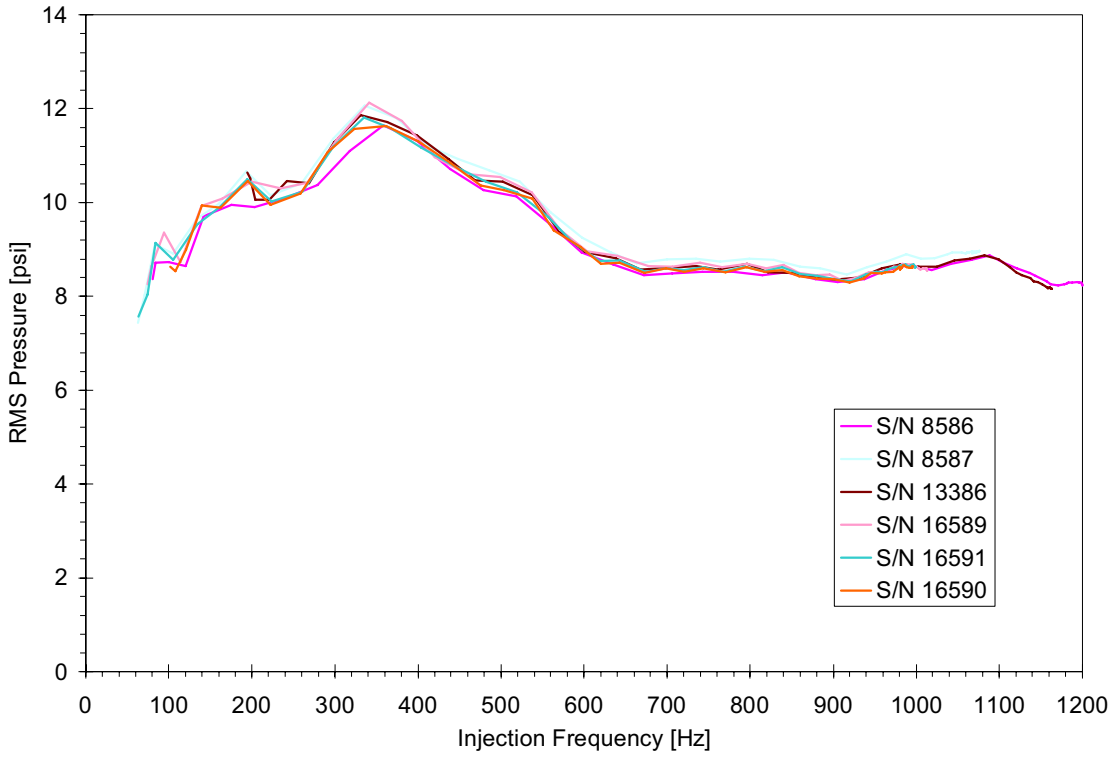

Figure 9: P2 RMS pressure v. injection frequency plot for air only at 1500 SLPM.

Calibration was also conducted for the thrust balance used in these experiments. The voltage reading across the linear potentiometer needed to be converted to the proportional thrust generated by the model. In order to determine this calibration coefficient, a series of known weights were placed over the exit of the combustion volume, without the presence of any flows, at approximately one-pound increments, and then were removed in the same order. The voltage reading was recorded for each weight placed on or taken off the model. This procedure was conducted several times to ensure repeatability. Figure 10(a) is a plot of the data collected from these tests. Each set of tests is distinguished by a different symbol.

From these tests, the calibration of the linear potentiometer was set to 10.0 lb/V, with a calculated uncertainty factor of $\pm 7\%$. An offset of -24.65 V was needed to "zero" the initial voltage reading from the linear potentiometer. Although the thrust balance would normally be restored to its initial position once weights were removed, a small amount of friction still exists in the system, which explains the scatter of data points in Figure 10(a). Figure 10(b) is an example plot of the thrust generated during a 10-second test run with reactant a flow rate of 1125 SLPM/air – 450 SLPM/H_2 at an approximate fixed frequency of 300 Hz. The red triangles on the plot represent the start and end of combustion. As shown, the linear potentiometer quickly responds to changes in thrust and only requires ~3 seconds to reach a steady state.

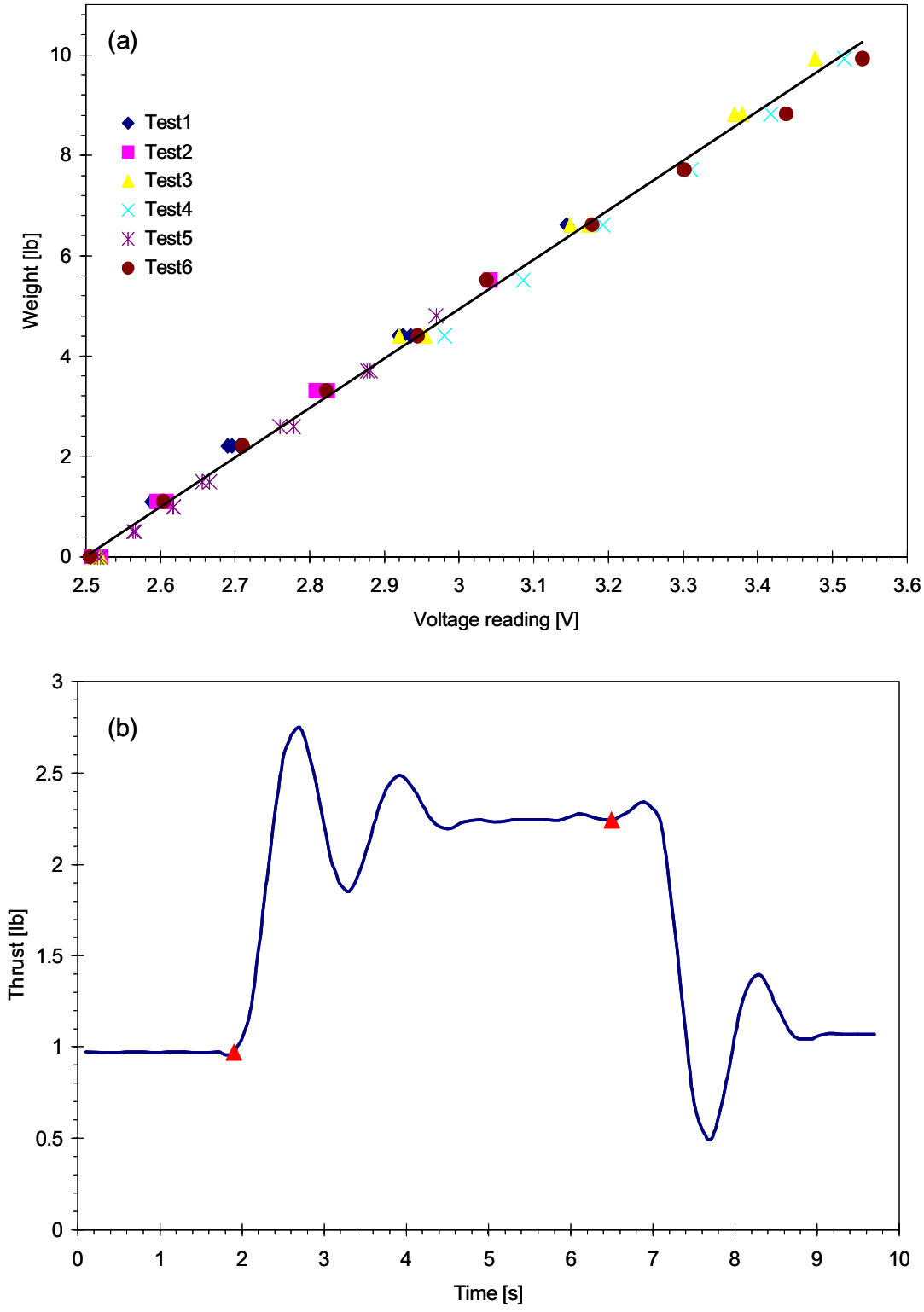

Figure 10: (a) Calibration data for thrust balance: weight v. voltage; (b) Example plot of thrust v. time: 1125 SLPM/air, 450 SLPM/ H_2 at 300 Hz.

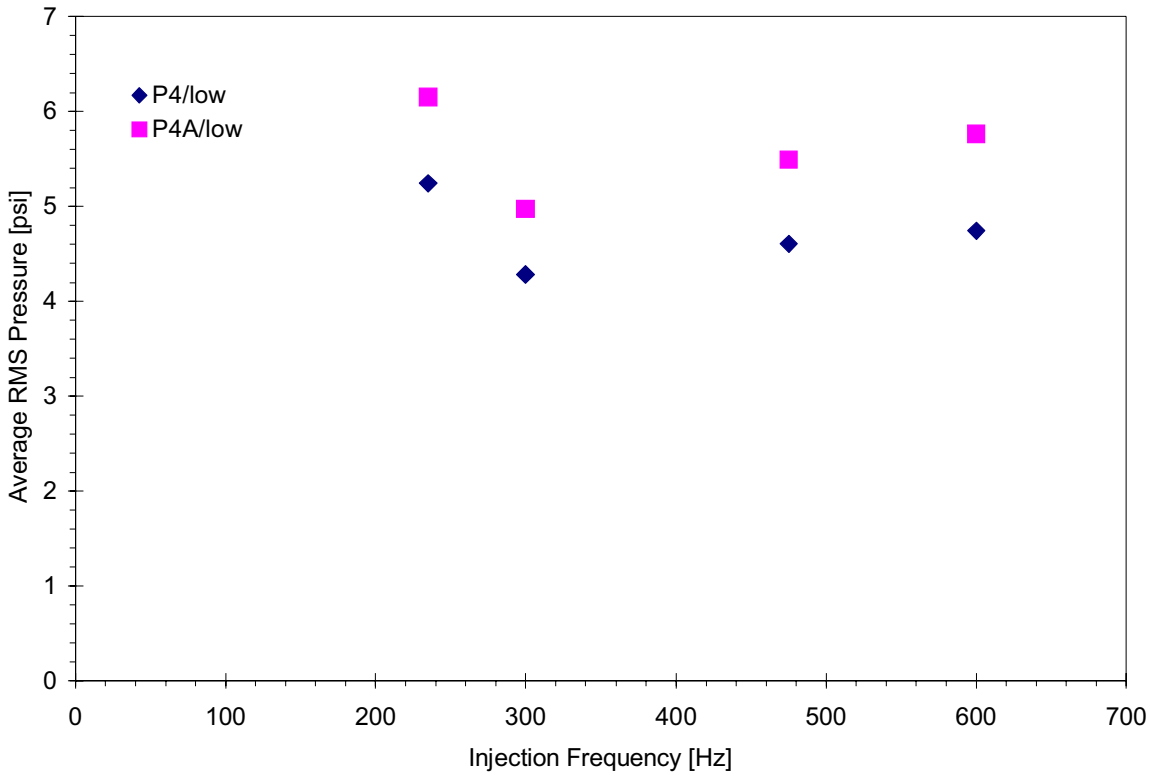

Figure 11: Average RMS pressure at the exit for 750 SLPM/air-300 SLPM/H_2 at various injection frequencies.

Simultaneous pressure data with two reactant flow rates – a low flow rate of 750 SLPM/air-300 SLPM/H_2 and a high flow rate of 1500 SLPM/air-600 SLPM/H_2 – at four fixed frequencies – 235, 300, 475, and 600 Hz – were collected to compare the time response of the two pressure taps located at the exit, P4 and P4A. (Recall that the diameter of the pressure taps is 0.076", except for P4A which has a diameter of 0.109".) These test runs lasted only one second, with a rate of 250,000 samples per second, to allow for better resolution of the pressure data collected. Figure 11 shows the average RMS pressure at each injection frequency for the low flow rate. As shown in Figure 11, average RMS pressure for the P4A is approximately 19% (~1 psi) greater than that of P4.

Data for test runs with a high flow rate are not presented in Figure 11 because the pressure sensor at the P4A location failed completely. This sensor was no longer used for subsequent runs. It is expected that average RMS pressure at the high flow rate would follow the same trend as at the lower flow rate, in that average RMS pressure from P4A would be approximately 19% larger than that at P4. It is important to note that gauges installed in the P4A location did not fair too well in experimental runs due to high heating. If this were not the case, then all pressure taps would have been made the same size.

Figure 12 is a portion of the pressure time history, for 750 SLPM/air-300 SLPM/H_2 at ~600 Hz injection frequency. The width of the pressure pulse for both pressure sensors is roughly the same regardless of the size of the pressure tap. However, the amplitude of the pressure peak for P4A is larger than that of P4, which explains why the RMS pressure plotted in Figure 11 was larger for P4A. Examination of a large number of pulses leads us to conclude that, on average, the detonation pressure rise is 45% higher for the larger pressure

tap than the smaller. By assuming the pressure drop across the tap is inversely proportional to the square of the tap area (i.e., proportional to the square of the velocity of flow through the tap), and extrapolating to infinite tap area, the true pressure rise is estimated to be 60% higher than for the small tap. This error helps explain why the pressure pulses measured in the present experiment are significantly less in amplitude than the Chapman-Jouget prediction for stoichiometric H_2-air detonations. This will be discussed further in Section 4.1.

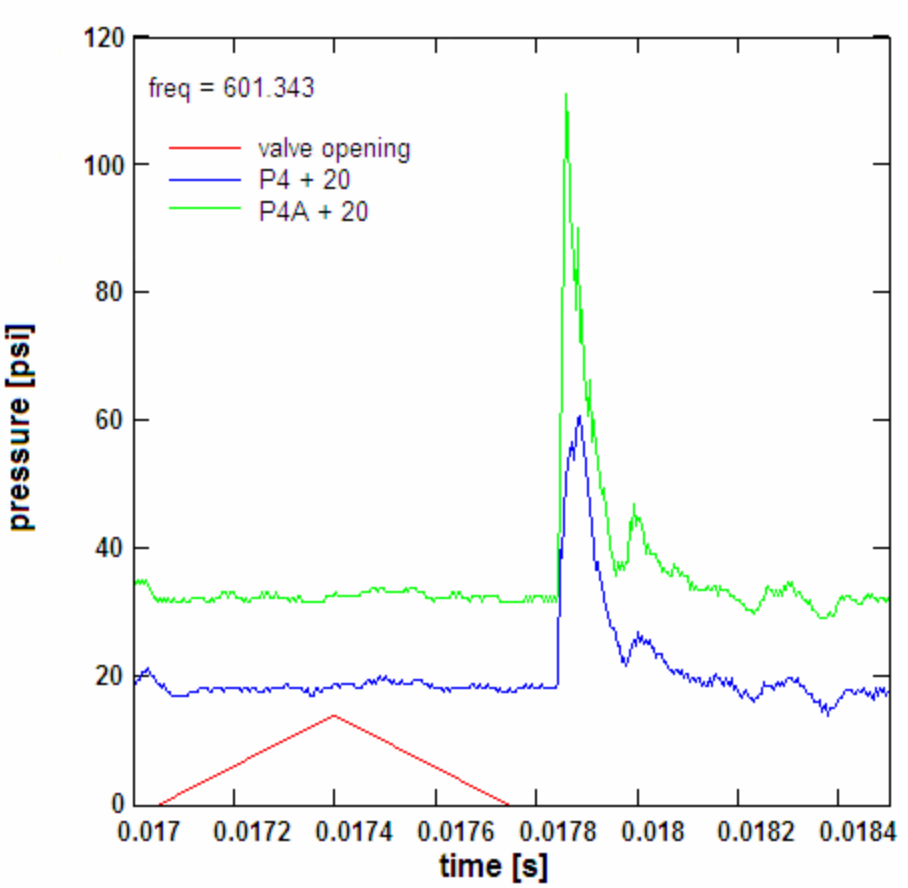

Figure 12: Segment of pressure time history for 750 SLPM/air-300 SLPM/H_2 at ~600 Hz.

Section 3.2 Gas Flow Rates and Supply Pressure

The high speed valve, described in Section 2.1 (Figure 1) contains no seals at the rotating shaft. There is a nominal 0.005 inch clearance between the shaft and the housing. Thus there is some leakage of, on one side, air, and on the other, hydrogen. The leakage air, having passed through the gap between shaft and housing, is vented through a port to the atmosphere. The leakage hydrogen passes through ball bearings (which are open and provide little restriction), and is discharged through tubing into the vent stack. The leakage flows were previously assumed small [2][15], and neglected. However, some significant time after to the experiments described in this report, the rates of leakage flow were measured (or estimated). In one experiment, a flow meter was placed in line with the hydrogen leakage and the flow was directly measured. It was not possible to measure the air leakage directly, but, in a separate experiment, air was flowed in both the air and the hydrogen supply lines at

the same pressure, and air leakage on the hydrogen side was measure. Care was taken to avoid flow restrictions in this case, other than between the shaft and housing, to make the hydrogen and air side as alike as possible. The valve was rotated normally during these tests (rotation speed had little effect on the leakage, provided rotation speed was not zero). It was found that the air leakage was 11% of the total air flow (flow delivered to the detonation tube was 89%); for hydrogen the leakage flow was 12% (flow to the tube was 88%). Uncertainty in H_2 leakage is ±6SLPM; for air it may be ±3% of the total air. Note that all flow rates specified elsewhere in this report, and previously [2][15], are total flow rates, inclusive of leakage, not flow rates to the tube.

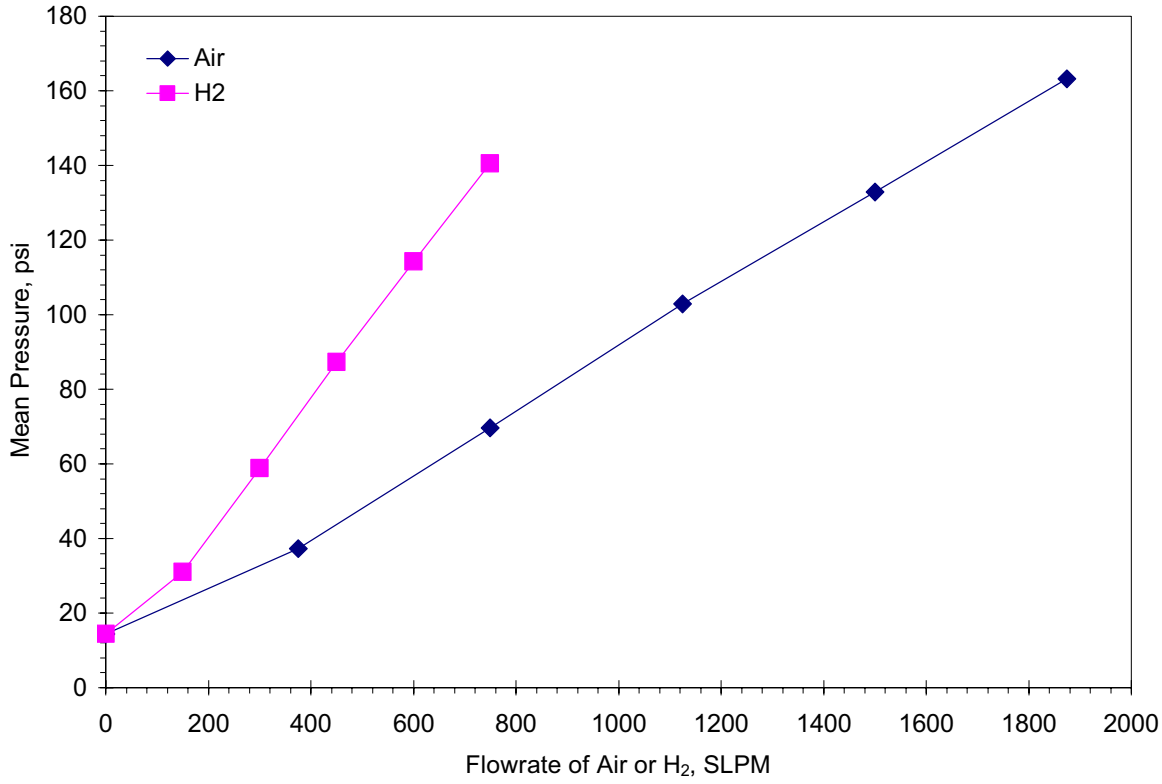

Figure 13: Plot of mean pressure of reactant supply flows v. flow rate.

As described in Section 2.3, pressure transducers were used to collect simultaneous mean pressure data in the valve plenum for H_2 and air supply flows. Figure 13 is a plot of this mean pressure data for reactant supply flows plotted against respective flow rates. As shown in Figure 13, mean pressures of the supply flows are rather high (~160 psi). This high pressure is necessary to inject the reactant flow at a significant velocity through the small orifices of the high-speed valve. The high-speed valve used in the present experiment was not developed to minimize pressure losses. A practical pulsed detonation actuator would have a valve optimized to minimize pressure losses (i.e., larger valve minimum areas), and, as a result, would be able to operate at lower supply pressures. However, devices such as the one presented here will always have a significant pressure drop in the injection of reactants because reactant flow is injected at a significant velocity. This is contrasted against a conventional PDE, where injection velocities are smaller and in principle, the valve could be

designed with lower pressure drops.

Section 3.3 Test Conditions

Several types of experimental runs were conducted for the present project. The first set of runs was done to measure pressure at the three locations in the combustion volume at various reactant flow rates, scanning a number of injection frequencies for five seconds. The second set of tests consisted of 10-second runs to measure the thrust generated at various reactant flow rates. Other types of tests involved collecting pressure data for one second at fixed frequencies and/or examining the role of spark firing during combustion.

For the first set of runs, several reactant flow rates were tested, scanning a number of injection frequencies during a 5-second test. For these experiments, reactant flow rates (inclusive of leakage flow - Section 3.2) studied include

- air only (no combustion) – 375, 750, 1125, and 1500 SLPM/air
- a stoichiometric mixture of air and H_2 – 375, 750, 1125, 1500, and 1875 SLPM/air with 150, 300, 450, 600, and 750 SLPM/H_2, respectively
- O_2-enriched air and H_2
- several fuel-lean conditions, in which air flow rate was kept constant, but H_2 flow rate was decreased.

The O_2-enriched cases were conducted to determine if combustion is complete in the actuator, and to determine if the performance is limited by reaction rate. In the stoichiometric case, there is exactly enough O_2 present in the air to completely consume the H_2, assuming that H_2 and air mix perfectly; however, the addition of O_2 to the airflow may help the H_2 to be consumed more completely in cases where H_2 and air alone do not mix perfectly. Another effect of O_2 addition is to increase the rate of reaction. During these runs, 10% of airflow was replaced with O_2, with H_2 flow rate kept the same as in the cases with a stoichiometric mixture of air and H_2. Results with O_2-enriched air and H_2 were compared to the stoichiometric cases. If stoichiometric H_2 and air mix perfectly, and all the H_2 reacts, then the cases with added O_2 should yield the same heat release, thrust, and RMS pressure. Increase in RMS pressure in cases with added O_2 would indicate that the H_2 was not all reacted for cases without O_2 addition, and is now reacting more completely. If the differences between the stoichiometric mixture and the O_2-enriched mixture are small, then it can be assumed that the reaction of H_2 is complete with or without the additional O_2.

For the fuel-lean conditions, testing started with 1875 SLPM/air – 700 SLPM/H_2. Flow of H_2 was reduced in increments of 50 SLPM until the reactants did not burn properly anymore, which occurred at 500 SLPM/H_2.

The second set of runs was to measure the thrust of the actuator model at specific frequencies for various reactant flow rates. Five stoichiometric fuel flow rates – 375, 750, 1125, 1500, and 1875 SLPM/air with 150, 300, 450, 600, and 750 SLPM/H_2, respectively – and two fuel-lean conditions – 1875 SLPM/air with 600 and 650 SLPM/H_2 – were chosen to be run at various fixed frequencies. The injection frequencies chosen for these runs were chosen to include peaks in RMS pressure derived from data collected during the five-second runs, including the resonant frequency and half the resonant frequency. During a typical run,

the valve motor was started and the injection frequency was established simultaneously with the flow rates for both H_2 and air. Data acquisition is initiated. Three seconds pass before the spark is ignited, which fires continuously at 120 Hz for approximately five seconds, and then is stopped. The three- and five-second delays allow the thrust balance to stabilize to allow a steady thrust measurement first without and then with combustion. The entire run lasts ten seconds, after which data is downloaded from the oscilloscope to the PC. Pressure data was not taken for the ten-second runs because the sample rate of the oscilloscope was not high enough to resolve the detonation peaks for runs longer than 5 seconds, and to preserve the gauges.

Several one-second experimental runs were conducted at various reactant flow rates and fixed injection frequencies. Procedure for these runs was similar to the five-second runs; however, injection frequency was fixed manually using the motor controller and data was only collected for one second during combustion. These tests were conducted in order to acquire a higher temporal resolution of the pressure data during combustion.

Also, five-millisecond experimental runs were conducted to observe the role of spark firing during combustion. Procedure for these runs was similar to the five-second runs; however, injection frequency was set manually using the motor controller, and data was only collected for 5 ms. Spark firing was displayed on Channel 4 of the oscilloscope. These experimental runs lasted only 5 ms to properly resolve the sparks, which were of very short duration.

During all tests, ambient temperature and pressure did not deviate significantly from standard atmospheric conditions, 20°C and 14.7 psia. Values of ambient temperature and pressure were collected with data acquisition, as well as the flow rates, temperature, and pressure for the supply flows of air, H_2, and O_2.

Section 3.4 Data Reduction and Analysis

Data from the digital oscilloscope contained data points from 4 channels with 250,000 samples per channel, collected over 5 seconds: Channel 1 from the valve shaft position photodiode, Channels 2, 3, and 4 from pressure sensors at P2, P3, and P4, respectively. Signals from Channels 2, 3, and 4 were converted from voltage signals to pressure readings in psi. Similar to previous work [2][15], each data string was processed and analyzed using a previously written data reduction program written using MathCAD software. Data was broken into 0.1 second segments of 5000 samples per channel for reduction. A/D data from the SC-2345 contains data for 14 channels at 1000 samples per second per channel, which is broken into 0.1 second segments of 100 samples per channel.

Channel 1 photodiode data, which contains a string of pulses of finite width, was processed to obtain a string of delta functions corresponding to the leading edge of each pulse, occurring once per shaft revolution. Injection frequency was obtained from the first maximum of the Fast Fourier Transform (FFT) of the processed Channel 1 signal, and then doubled to convert shaft revolution frequency to valve opening frequency, since valve opening and injection of reactants occurs twice per shaft revolution. Phase delay between valve opening and photodiode signal needed to be determined because the signal from the photodiode that collects light from a reflective strip on the rotating shaft is at an arbitrary, but

fixed, phase in relation to the valve opening. A correction constant was determined in a separate experiment in which the valve was removed from the actuator and operated with a pressure sensor connected to the valve exit. The corrected valve opening is plotted with the pressure traces collected from Channels 2, 3, and 4.

Pressure data from Channels 2, 3, and 4 were analyzed to obtain two separate results. First, short time standard deviation of pressure (RMS pressure) for each 0.1 second segment was computed. The second analysis, which required a number of steps, computed the one-cycle-delay correlation coefficient for each segment. This correlation coefficient was obtained by shifting the data segment one reactant injection cycle and then computing the correlation coefficient between the original unshifted and the shifted segment. When the correlation coefficient is one, this indicates perfectly periodic behavior at the injection frequency. Results for each segment of the data from Channels 2, 3, and 4 could be cross-plotted with the valve frequency obtained from Channel 1 data or with time into the test.

Chapter 4 - Experimental Results and Discussion

Section 4.1 Pressure Time History Results

Pressure time history data were reduced as described in Section 3.4 to obtain RMS pressure (in psi) and one-cycle-delay correlation coefficient as a function of injection frequency. Results for various cases are shown and discussed in this section.

Cases with air only, i.e. no combustion, were conducted for two flow rates: 750 SLPM/air and 1500 SLPM/air. Results from these tests may be contrasted against cases with combustion to show the effects of combustion. Figure 14 shows results derived from pressure time history results for these two cases. Figure 14(a) and (c) correspond with 750 SLPM/air; Figure 14(b) and (d) correspond with 1500 SLPM/air.

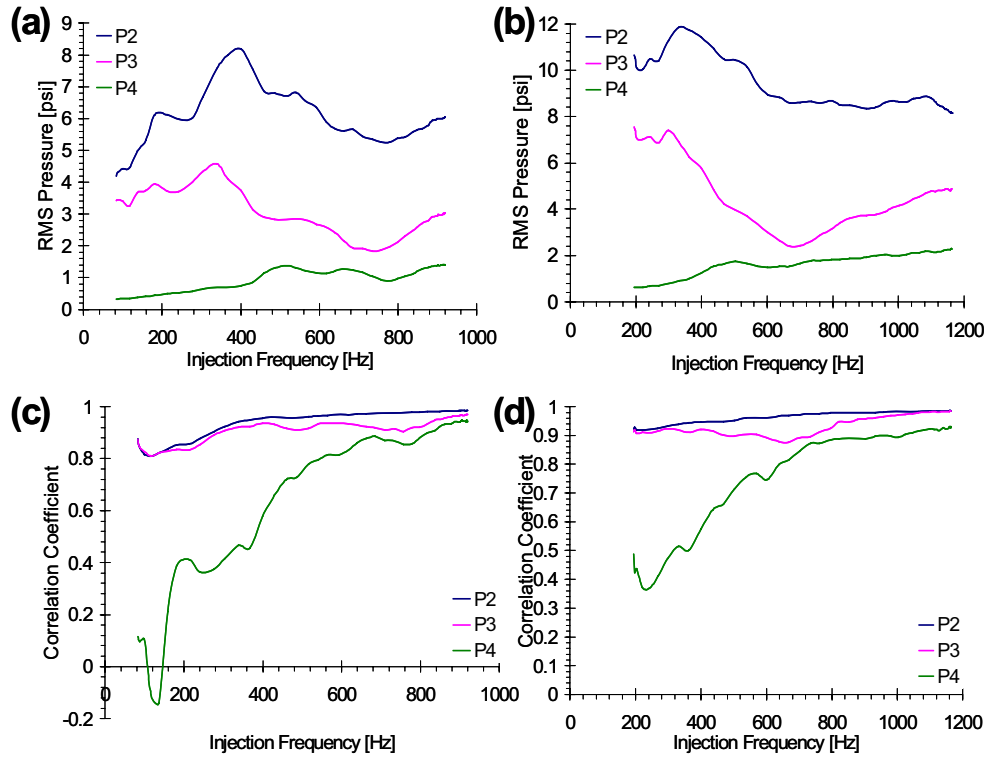

Figure 14: Response of actuator with air flow at 750 SLPM - (a), (c) - and 1500 SLPM - (b), (d). RMS pressures are given in (a), (b), and one-cycle-delay correlation coefficient are given in (c), (d).

RMS pressure fluctuations, shown in Figure 14(a) and (b), show that pressure fluctuation is highest at P2 and lowest at P4. RMS pressure followed this pattern for all experimental cases tested. This behavior is expected for the quarter wave ($\lambda/4$) mode of acoustic resonance, where the pressure fluctuation amplitude is greatest at the closed end of the tube and zero at the exit, and was also observed in the previous experiments [2]. Resonance, indicated by peaks in the pressure amplitude, appears to occur at approximately 400 Hz and 330 Hz for air flow rates of 750 SLPM and 1500 SLPM, respectively. These experimentally determined resonant frequencies have ratios to theoretical $\lambda/4$ resonant frequency (423.75 Hz – calculated using 1130 ft/s as the speed of sound in air) of 0.9440 and 0.7811, respectively. In Figure 14(a), a local pressure peak around 200 Hz occurs, indicating

strong pressure fluctuation at half the resonant frequency. As opposed to previous work [15], few resonant frequencies were identified based on the pressure time histories collected.

One-cycle-delay correlation coefficient is shown in Figure 14(c) and (d). As discussed in Section 3.4, when the correlation coefficient is one, the waveforms are perfectly periodic. Figure 14(c) and (d) indicate that the pressure fluctuations are almost perfectly periodic at higher frequencies.

Figure 15 shows three segments of the pressure time history for the case with airflow at 1500 SLPM. The pressure time history at 212 Hz in Figure 15(a) shows small and chaotic P4 pressure fluctuations, which corresponds to low RMS pressure and low value of correlation coefficient, as seen in Figure 14(b) and (d). P2 and P3 pressure fluctuations appear periodic and are consistent in amplitude and shape. At ~423 Hz, Figure 15(b), pressure fluctuations for all three gauges appear periodic. As injection frequency increases, Figure 15(c), pressure fluctuations remain periodic, but amplitude of the pressure peaks decreases slightly. Pressure fluctuations appear to remain consistent in amplitude and shape at each injection cycle at the highest frequency, Figure 14(d), corresponding to a correlation coefficient near one. Average P2 pressure amplitude, the difference between minimum and peak values, for flow at 1500 SLPM/air, as shown in Figure 15, is ~30 psi.

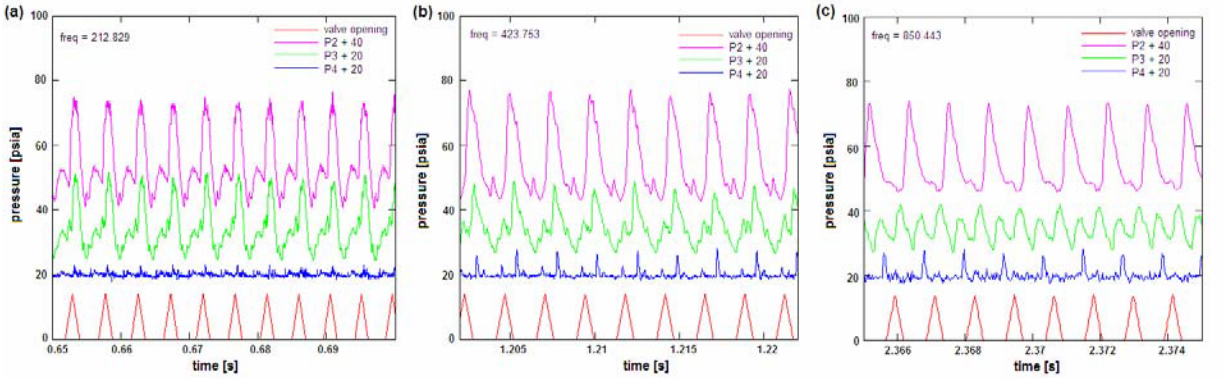

Figure 15: Three segments of pressure time history for airflow at 1500 SLPM: (a) 212 Hz, (b) 423 Hz, (c) 850 Hz injection frequency.

As discussed in Section 3.4, valve opening, shown in red in Figure 15, is plotted with pressure traces collected from Channels 2, 3, and 4. During the up- and down-slope of the valve opening trace, only a fraction of the flow passages in the rotating shaft of the high-speed valve are open to the corresponding passages in the valve housing assembly. At the peak of the valve opening trace, passages are perfectly aligned, allowing for maximum injection of reactants.

Figure 16 shows results derived from pressure time history results for two cases in which combustion does occur. Figure 16 (a) and (c) correspond with 750 SLPM/air – 300 SLPM/H_2; Figure 16 (b) and (d) correspond with 1500 SLPM/air – 600 SLPM/H_2. Compared to Figure 14(a) and (b), RMS pressure has increased significantly as a result of combustion, which is to be expected.

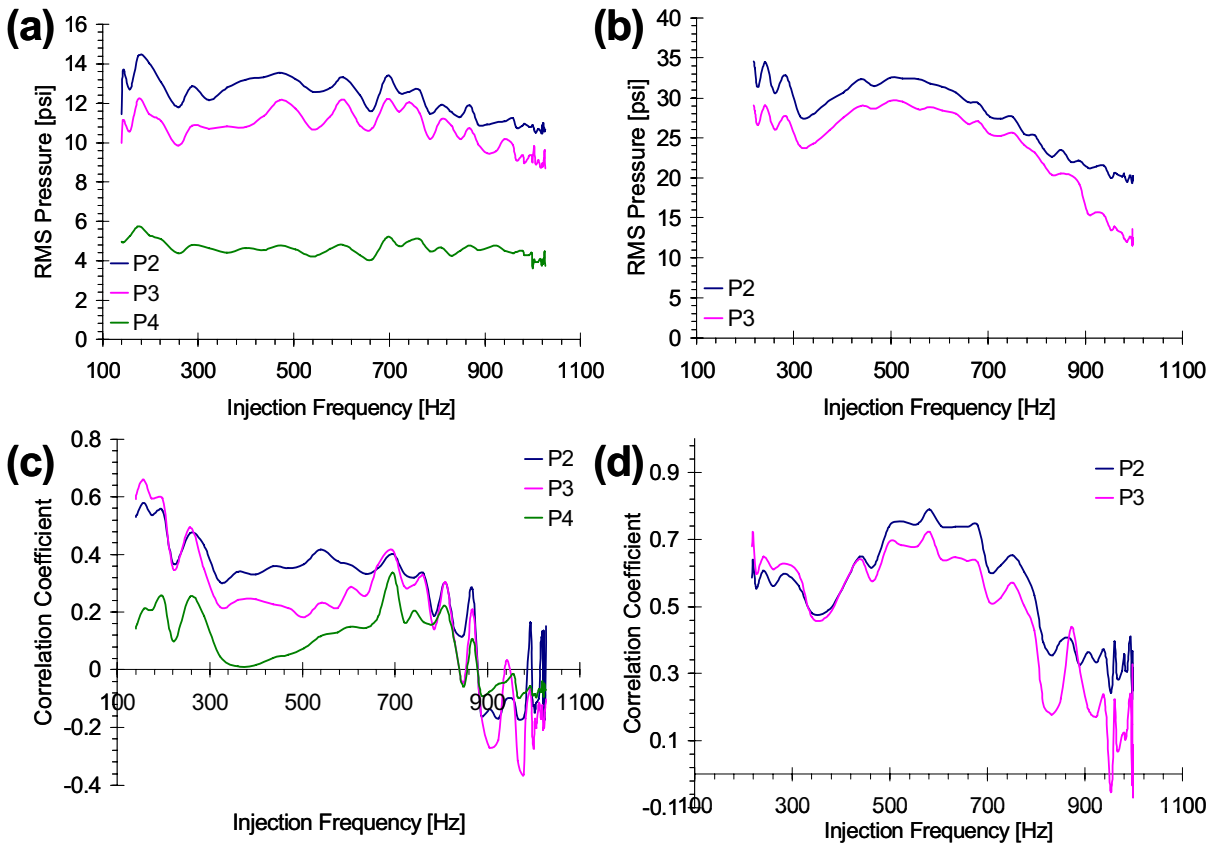

Figure 16: Response of the actuator with combustion at 750 SLPM/air-300 SLPM/H_2 - (a), (c) - and 1500 SLPM/air-600 SLPM/H_2 - (b), (d). RMS pressures are in (a), (b), and one-cycle-delay correlation coefficient in (c), (d).

Another effect of combustion is that the $\lambda/4$ mode resonant frequency has increased from ~400 Hz to ~600 Hz. Resonance is identified as the frequency at which the pressure fluctuations are the highest and the waveform the most periodic, and the mode by inspection of the amplitude and relative phases of waveform. This is consistent with previous work [15], in which the resonant frequency was found to increase less than expected based on the higher speed of sound in the combustion products. The speed of sound in combustion products is 3200 ft/s, compared to 1130 ft/s in air. Using this new speed of sound, the theoretical resonant frequency is calculated to be 1200 Hz, which is double the experimentally obtained resonant frequency of 600 Hz. This discrepancy must be due in part to the presence of unburned reactants with lower speed of sound in the tube during much of the detonation cycle. More generally it is due to the combination of non-linear processes occurring during detonation (i.e., formation and propagation of the shocks, variable composition, and chemistry of the reactants) which affect the wave propagation speed. The present work does not include results for injection of reactants at a frequency of 1200 Hz; therefore, it cannot be said that resonance does not occur at this injection frequency. Previous work with the second generation model has shown that waveforms are chaotic at ~999 Hz but periodic again at ~1401 Hz [2]; however, these waveforms were consistent with the $3\lambda/4$ mode, and combustion was by deflagration not detonation.

Figure 17 shows segments of pressure time history for reactant flow at 750 SLPM/air-

300 SLPM/H_2, (a) and (b), and 1500 SLPM/air-600 SLPM/H_2, (c) and (d), at two injection frequencies, ~285 Hz and ~600 Hz. At the lower flow rate, Figure 17 (a) and (b), it is evident that a detonation does not occur at each injection cycle. Also, P2 pressure amplitudes vary for each detonation that occurs. Non-periodic behavior of the detonations corresponds with the low value of correlation coefficient shown in Figure 16(c).

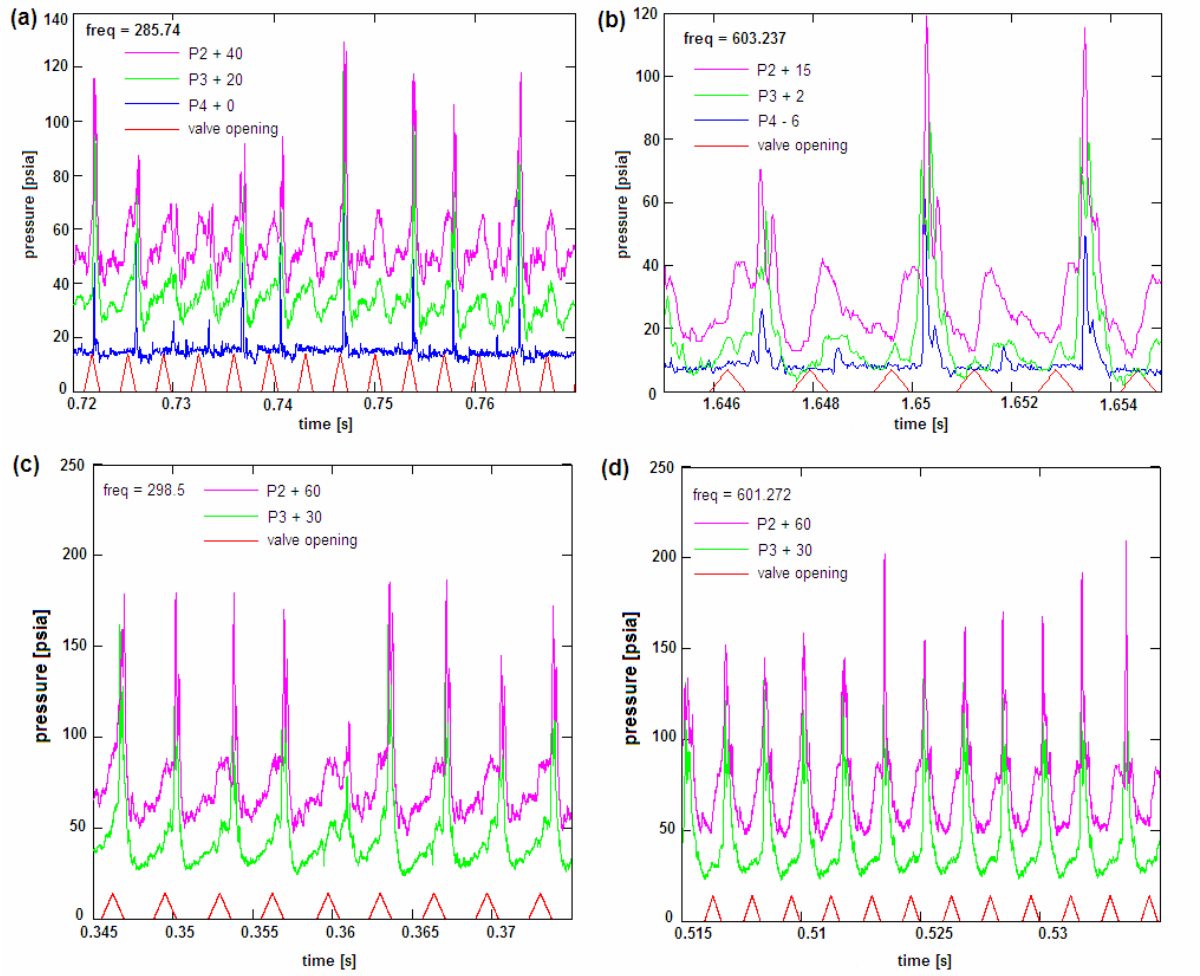

Figure 17: Segments of pressure time history for combustion: 750SLPM/air-300SLPM/H_2 – (a) 285 Hz, (b) 603 Hz; 1500 SLPM/air-600 SLPM/H_2 – (c) 298 Hz, (d) 601 Hz injection frequency.

At the higher flow rate, Figure 17 (c) and (d), detonations occur at almost every injection cycle. Detonations appear to be strong with average P2 pressure amplitudes ~125 psi at ~300 Hz, Figure 17 (c), and ~138 psi at ~600 Hz, Figure 17 (d). The pressure amplitude is defined as the difference between minimum and peak values in a cycle. As mentioned previously in Section 3.1, there is a bias error in the pressure measurements due to the small size of the pressure taps. This bias error results in the pressure amplitude of detonations being measured roughly one half their true value. Thus, true amplitudes of the pressure fluctuations are likely over ~200 psia. The C-J prediction for detonations of stoichiometric H_2 and air at 1 atm is 168 psia [2]. However, in reality the pressure in the combustion tube is oscillating around atmospheric pressure, and at the moment of detonation is higher than 14.7 psia. Since the C-J pressure just after detonation is expected to roughly

scale with the pressure just prior to it, the pressure after detonation is expected to be greater than 168 psia. Although there are large uncertainties, it appears that the actual pressure amplitudes in the combustion tube are roughly consistent with C-J detonations.

At ~300 Hz, Figure 17 (c), amplitude and shape of each pressure fluctuation are not very consistent, which is why the correlation coefficient is not very close to one. At ~600 Hz, Figure 17 (d), the pressure fluctuations are a little more consistent, which corresponds to a local peak in the correlation coefficient found in Figure 17 (d). Compared to Figure 15, which shows the pressure time history for airflow only, Figure 17 shows the effects of combustion on the pressure waveform. Consider Figure 17 (d), which shows strong, periodic detonations occurring at the resonant frequency. Amplitude of the pressure fluctuation is three times that with air only (and, in reality, probably more given the bias error in the gauges). Also, detonations occur at the peak in pressure of the underlying $\lambda/4$ mode, unlike at half the resonant frequency, in Figure 17 (c), where detonations occur just after the peak, causing a small "hump" in the waveform just before the detonation.

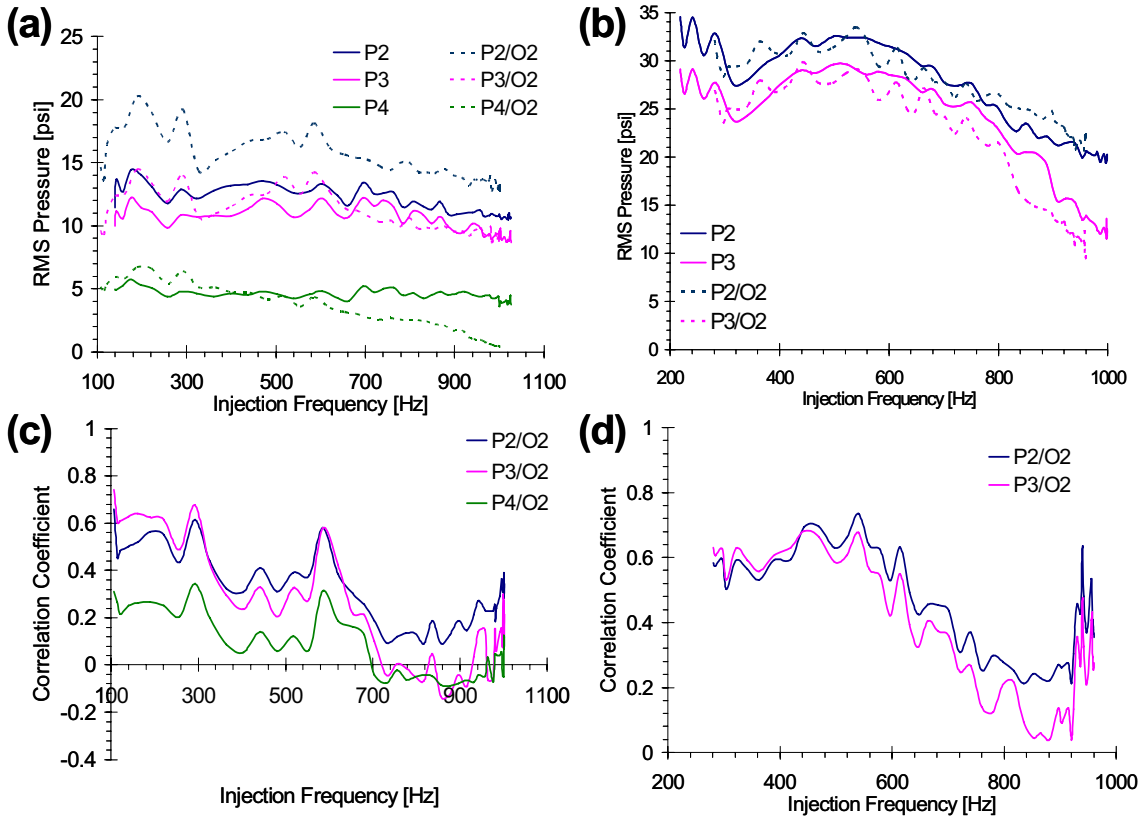

Figure 18: Response of the actuator with O_2-enriched combustion at 75 SLPM/O_2-675 SLPM/air-300 SLPM/H_2 - (a), (c) - and 150 SLPM/O_2-1350 SLPM/air-600 SLPM/H_2 - (b), (d). RMS pressures are in (a), (b), and one-cycle-delay correlation coefficient in (c), (d).

As discussed in Section 3.3, tests were conducted replacing 10% of the air flow with O_2. Figure 18 shows results derived from pressure time history results for two cases: Figure 18(a) and (c) correspond with 75 SLPM/O_2 – 675 SLPM/air – 300 SLPM/H_2; Figure 18(b) and (d) correspond with 150 SLPM/O_2 – 1350 SLPM/air – 600 SLPM/H_2. RMS pressures plotted in Figure 18(a) and (b) also include RMS pressure for baseline combustion runs

without additional O_2, previously plotted in Figure 16(a) and (b), for comparison.

For the lower flow rate, Figure 18(a), introduction of O_2 into the reactant mixture increased RMS pressure fluctuations from gauge P2 by ~40% at lower injection frequencies and ~25% at higher injection frequencies. Similarly, P3 RMS pressure fluctuations increased ~20% at lower injection frequencies, but no significant changes are noticed at high frequencies or in P4 RMS pressure fluctuations. This increase in RMS pressure reaffirms the fact that reacion was not complete at this low flow rate without the addition of O_2.

For the higher flow rate, Figure 18(b), the addition of O_2 in the reactant mixture does not significantly change the RMS pressure for any of the gauges. This indicates that mixing and combustion of the reactant mixture was complete without the addition of O_2. Also, RMS pressure fluctuations for the O_2-enriched cases appear to peak at similar injection frequencies as the normal combustion cases, indicating that there is no change in the resonant frequency when O_2 is introduced into the reactant mixture. The correlation coefficient, Figure 18(c) and (d), appears to be approximately unchanged compared to Figure 16(c) and (d).

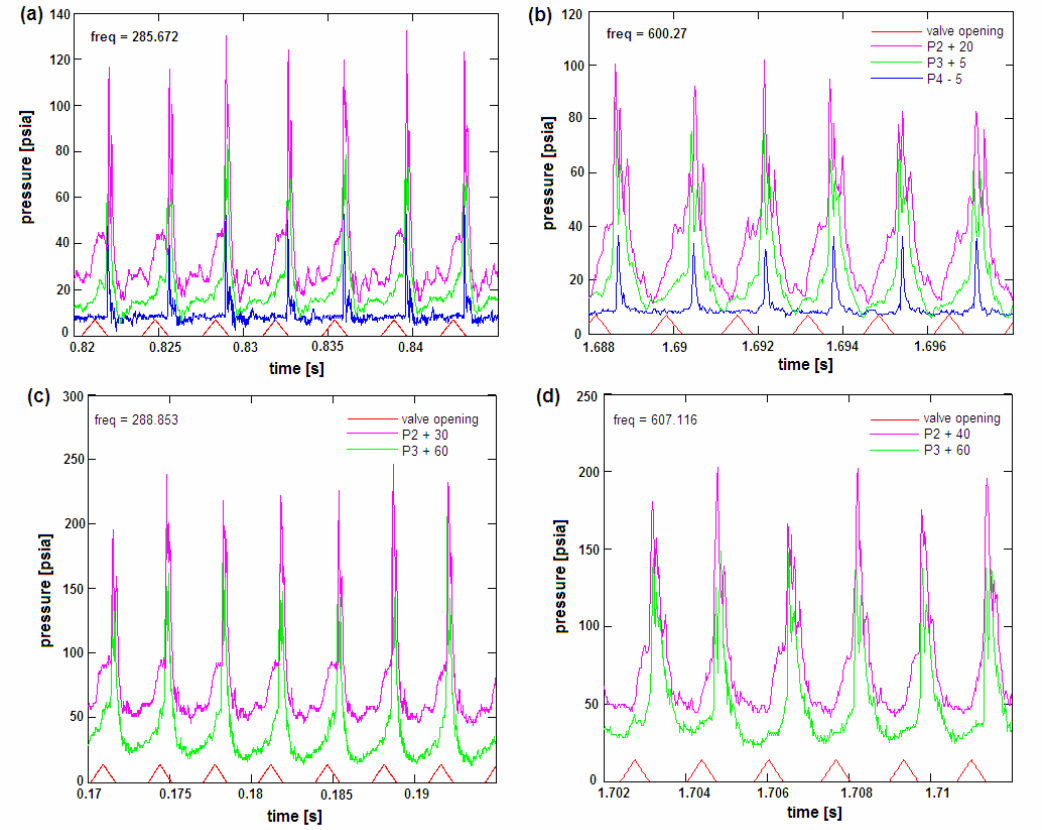

Figure 19: Segments of pressure time history for combustion: 75 SLPM/O_2-675 SLPM/air-300SLPM/H_2 – (a) 285 Hz, (b) 600 Hz; 150 SLPM/O_2-1350 SLPM/air-600 SLPM/H_2 – (c) 288 Hz, (d) 607 Hz injection frequency.

Figure 19 shows pressure time history segments for flow at 75 SLPM/O_2-675 SLPM/air-300 SLPM/H_2, Figure 19(a) and (b), and 150 SLPM/O_2-1350 SLPM/air-600 SLPM/H_2, Figure 19(c) and (d). It is obvious again that the introduction of O_2 into the reactant mixture has enhanced combustion at the lower flow rates, Figure 19(a) and (b), since distinct, periodic detonations occur at each injection cycle and have average P2 pressure

amplitudes of ~100 psi at ~285 Hz, Figure 19(a), and ~75 psi at ~600 Hz, Figure 19(b).

Compared to the corresponding case, shown in Figure 17 (a) and (b), pressure amplitudes are much larger and more consistent in value and shape. This corresponds to peaks in the correlation coefficient, Figure 18(c), at ~285 and ~600 Hz. At the higher flow rate, detonations occur at each injection cycle, as in the baseline case, with average P2 pressure amplitudes of ~160 psi at ~285 Hz, Figure 19(c), and ~140 psi at ~600 Hz, Figure 19(d). Compared to the corresponding case, shown in Figure 17 (c) and (d), average pressure amplitudes are nearly the same, but the pressure amplitudes for the O_2-enriched case do not fluctuate as much as in the stoichiometric case.

Figure 20 shows results derived from pressure time histories for three cases during which the experiments were conducted at fuel-lean conditions. The results presented are for 1875 SLPM/air and three H_2 flow rates: 750 SLPM (near-stoichiometric), 650 SLPM and 600 SLPM. Figure 20(a) shows that as the flow of H_2 is decreased, RMS pressure fluctuations also decrease. It appears as though RMS pressure fluctuations for the three cases, shown in Figure 20(a), peak at similar injection frequencies, with local peaks occurring at various injection frequencies: ~200, ~400, and ~600 Hz. Figure 20(b) shows that the correlation coefficient is moderately high for injection frequencies between 420 Hz and 750 Hz, with all three cases having local maxima at ~610 Hz.

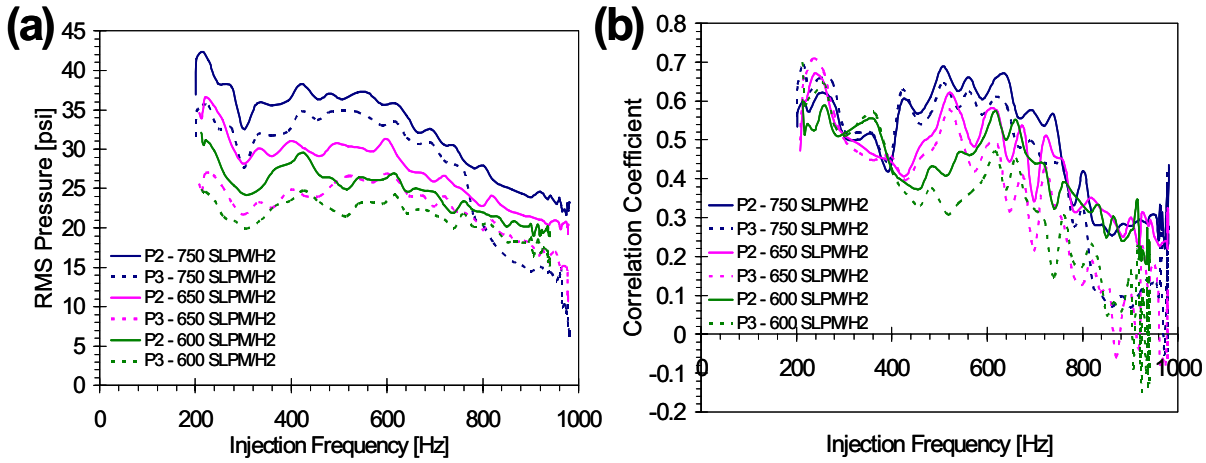

Figure 20: Response of actuator with fuel-lean combustion at 1875 SLPM/air and various flow rates of H_2. RMS pressures are in (a), and one-cycle–delay correlations coefficient in (b).

Figure 21 shows pressure time history segments for flow at 1875 SLPM/air with two fuel-lean cases and one stoichiometric case: 600 SLPM/H_2, Figure 21(a) and (b), 650 SLPM/H_2, Figure 21(c) and (d), and 750 SLPM/H_2, Figure 21(e) and (f). For each segment of pressure time history shown, detonations occur at each injection cycle. For the 600 SLPM/H_2 case, average P2 pressure amplitudes are ~132 psi at ~425 Hz, Figure 21(a), and ~100 psi at ~617 Hz, Figure 21(b). For the 650 SLPM/H_2 case, average P2 pressure amplitudes are ~160 psi at ~410 Hz, Figure 21(c), and ~130 psi at ~603 Hz, Figure 21(d). For the stoichiometric case of 750 SLPM/H_2, average P2 pressure amplitudes are ~173 psi at ~416 Hz, Figure 21(e), and ~163 psi at ~619 Hz, Figure 21(f). As expected, average P2 pressure amplitude increases with H_2 flow rate. The waveform shape, shown Figure 21, appears periodic and somewhat consistent in width in each segment shown, but variations in the shape of the waveform at

each cycle result in a correlation coefficient less than to one.

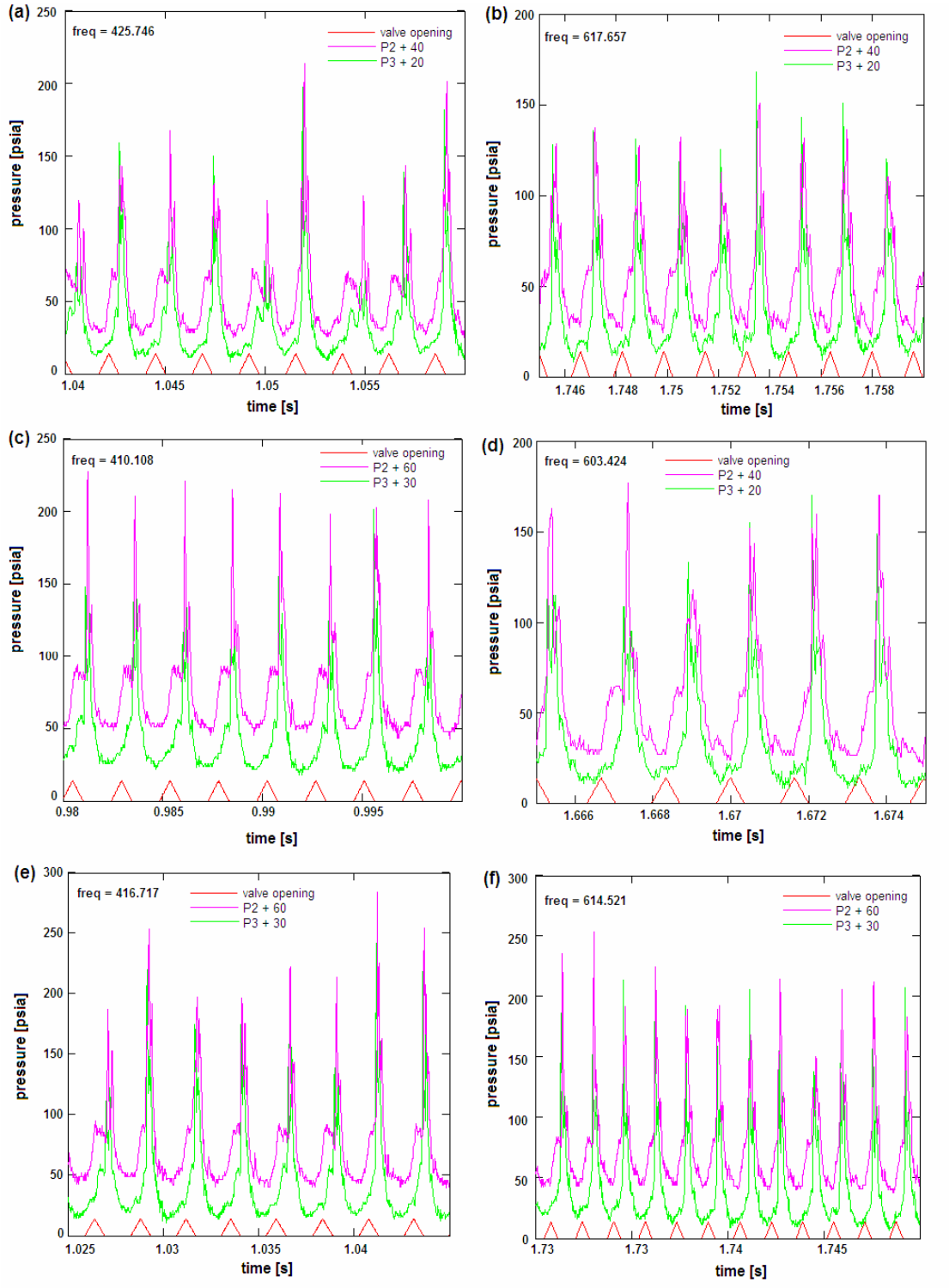

Figure 21: Segments of pressure time history for combustion: 1875 SLPM.air-600 SLPM/H_2 - (a) 425 Hz, (b) 617 Hz; 1875 SLPM/air-650 SLPM/H_2 – (c) 410 Hz, (d) 603 Hz; 1875 SLPM/air-750 SLPM/H_2: (e) 416 Hz, (f) 614 Hz injection frequency.

Section 4.2 Thrust Balance Results

As discussed in Section 3.3, thrust balance measurements were acquired at various reactant flow rates and injection frequencies. Figure 22 shows overall steady-state thrust for cases with combustion at various injection frequencies for a number of stoichiometric reactant flow rates. The thrust at any given flow rate is a maximum at the resonant frequency, ~600 Hz, except at the highest flow rate of 1875 SLPM/air-750 SLPM/H_2. At this flow rate, maximum thrust of 6.27 lb. occurs at ~525 Hz, but it is not significantly higher (only +3.64%) than the thrust measured at ~600 Hz, which is 6.05 lb.

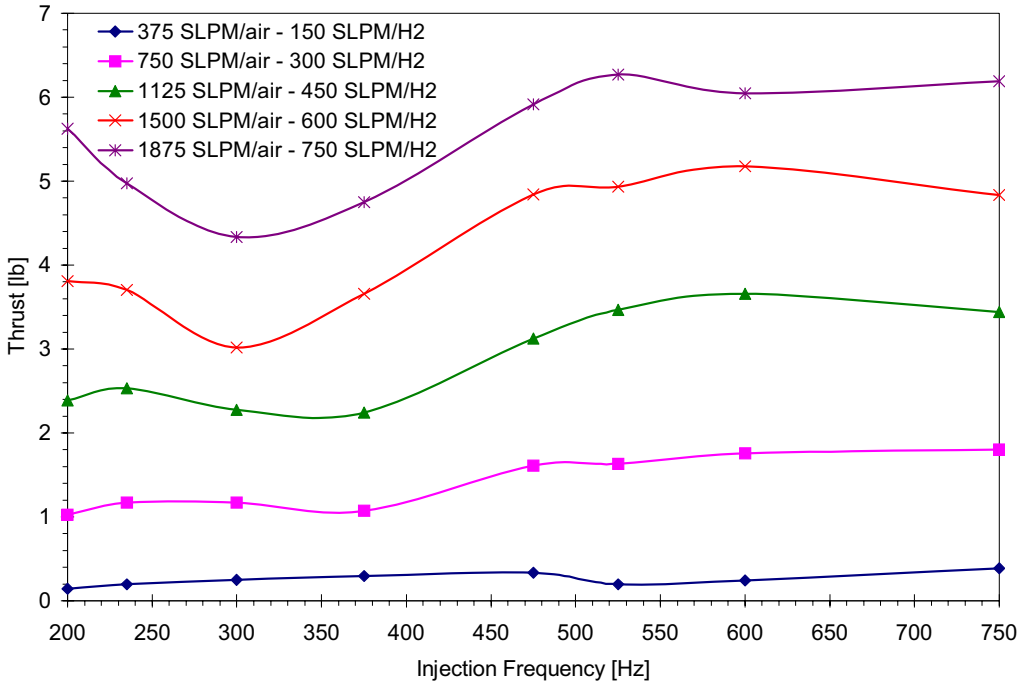

Figure 22: Overall steady-state thrust for various stoichiometric reactant flow rates.

Figure 23 is a plot of the steady state thrust generated by the reactant flow at various flow rates and injection frequencies, before igniting combustion. This thrust ranges between 0.1 to 1.7 lbs. As a percentage of the thrust with combustion, it ranges from as little as 7.8% to as much as 75%, both cases occurring at the lowest flow rate, 375 SLPM/air-150 SLPM/H_2. In general, the increase in thrust with combustion at the lowest flow rate is small because combustion is not complete. As the reactant flow rate is increased, the fraction of the thrust contributed by the reactant flows prior to combustion is reduced because the reaction tends to be more complete. At the resonant frequency of ~600 Hz, for flow rates greater than or equal to 750 SLPM/air – 300 SLPM/H_2, the thrust from the reactant flows alone is ~25% of the thrust measured with combustion.

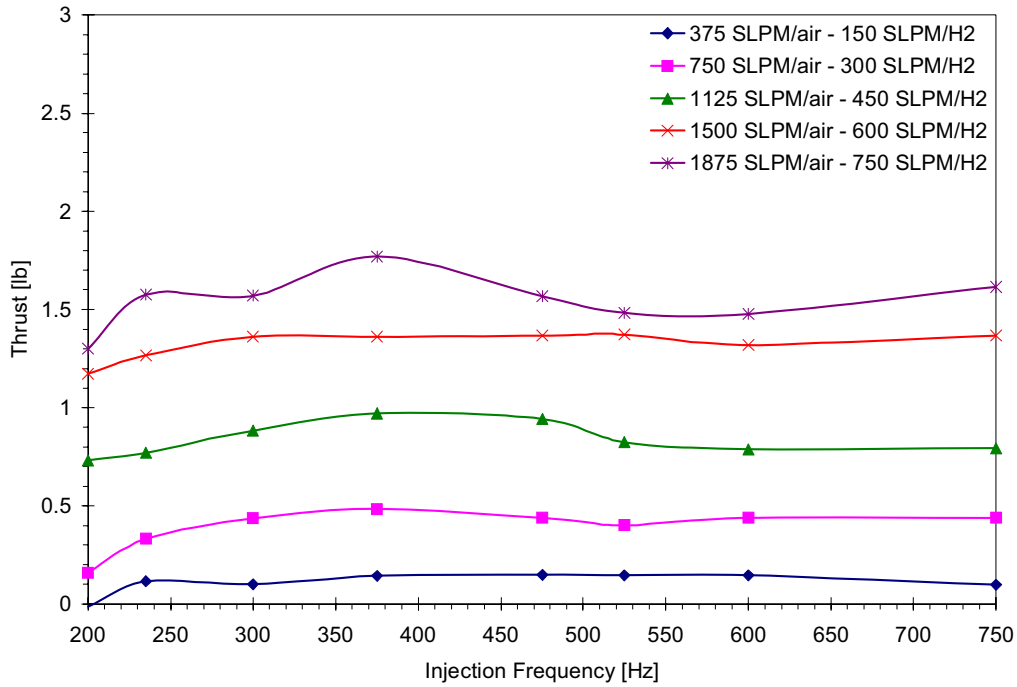

Figure 23: Steady-state thrust from presence of reactant flows at various stoichiometric flow rates.

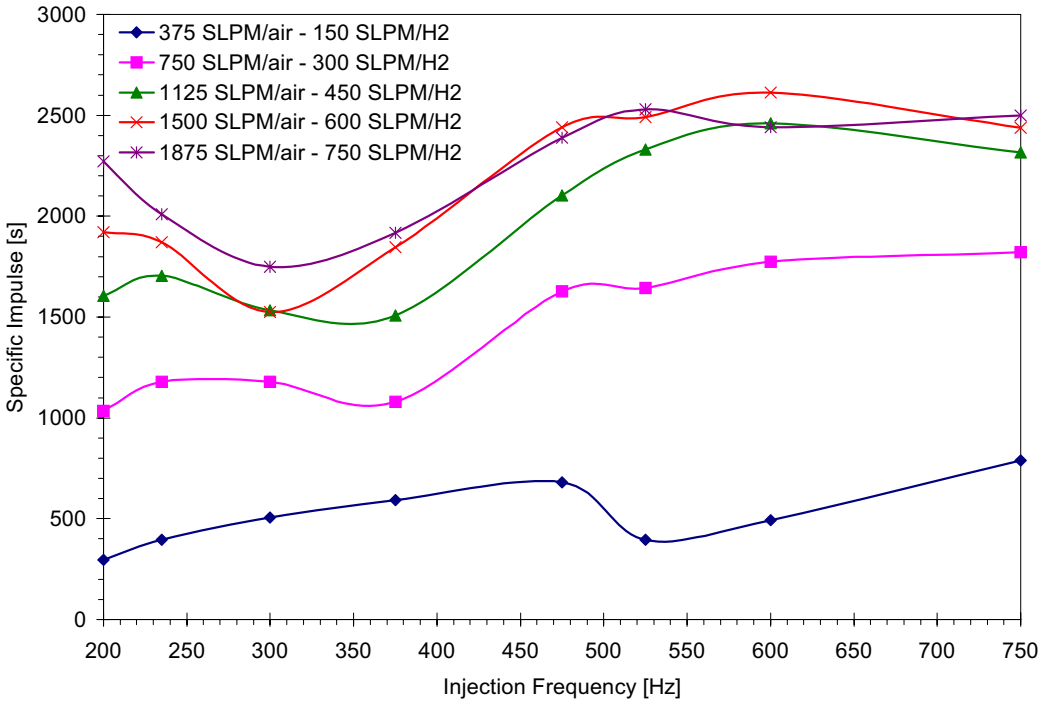

Figure 24: Steady-state specific impulse for various stoichiometric reactant flow rates.

Figure 24 is a plot of steady state specific impulse, I_{sp}, for various frequencies at a number of stoichiometric reactant flow rates. The I_{sp} plotted in Figure 24 is calculated from the thrust plotted in Figure 22. At the resonant frequency of 600 Hz, the I_{sp} of the three highest flow rates is approximately 2500 s. The close similarity between the three highest

flow rates is promising, indicating that combustion is complete at these flow rates and frequencies. At the lower flow rates, low I_{sp} is a result of incomplete combustion in the combustion volume.

Figure 25 is a plot of steady-state thrust with combustion, at various injection frequencies for three reactant flow rates: a stoichiometric reactant mixture of 1875 SLPM/air-750 SLPM/H_2 and two fuel-lean mixtures of 1875 SLPM/air-600 SLPM/H_2 and 1875 SLPM/air-650 SLPM/H_2. It is expected that thrust would be highest for the stoichiometric mixture and would decrease with the decrease in H_2 flow rate. This behavior is true at the higher injection frequencies, but the opposite trend is observed at the lower frequencies. Figure 24 shows that maximum thrust is ~5.5 lb for the 1875 SLPM/air-600 SLPM/H_2 case at ~300 Hz and ~5.9 lb for the 1875 SLPM/air-650 SLPM/H_2 case at ~425 Hz.

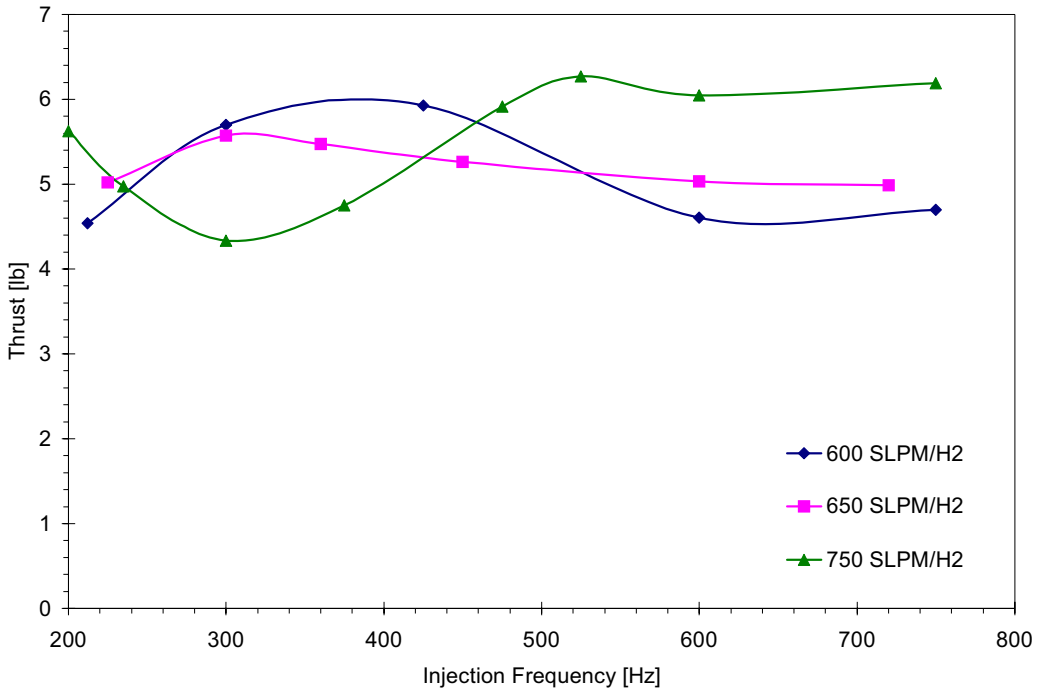

Figure 25: Steady-state thrust for various fuel-lean reactant flow rates.

Figure 26 is a plot of the I_{sp} calculated from the thrust plotted in Figure 25. I_{sp} differs greatly at the lower injection frequencies, which is a result of the inconsistent behavior of the thrust plotted in Figure 25. However, at ~600 Hz, the I_{sp} of the two fuel-lean cases shown is ~2400 s, which is similar to the three highest stoichiometric flow rates plotted in Figure 24. The explanation for this trend is not known. It is possible that there are two offsetting trends whose effect depends on frequency. On the one hand, a fuel-lean condition tends to reduce the reactivity of the reactants, which would be expected to reduce I_{sp}. On the other hand, fuel-lean increases the mass of the reactants per unit mass of fuel (H_2), similar to reducing the fill fraction, which in PDEs increases I_{sp} (see the discussions in Section 4.4). Further studies will need to be conducted in order to clearly understand the effects of operating fuel-lean.

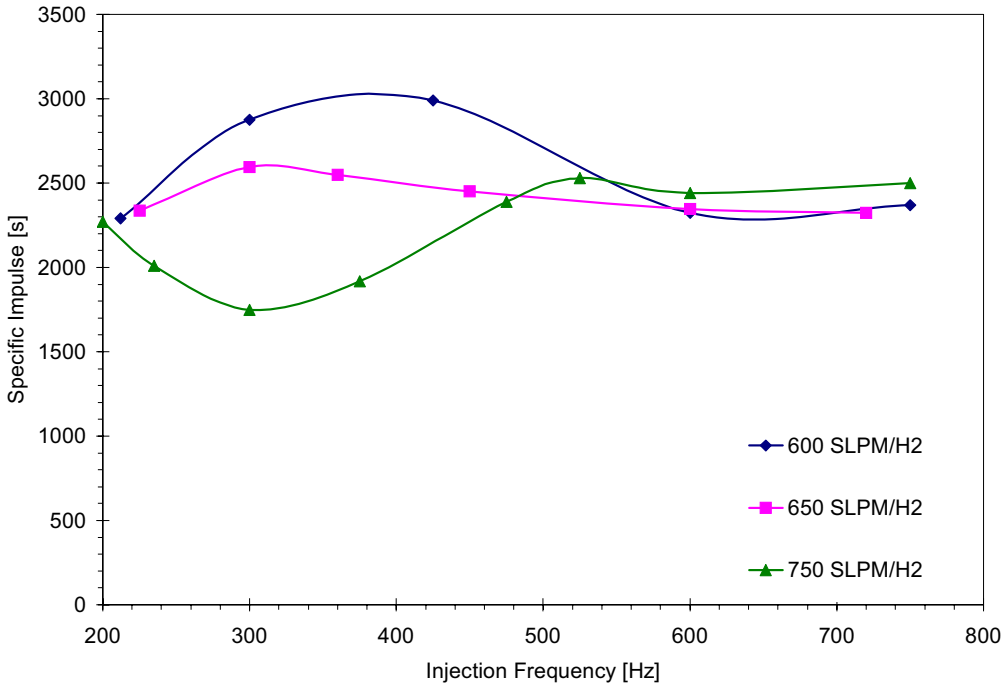

Figure 26: Steady-state specific impulse, from the flow of fuel and combustion, for various reactant flow rates: 1875 SLPM/air with 600, 650, and 750 SLPM/ H_2.

Section 4.3 Role of Spark

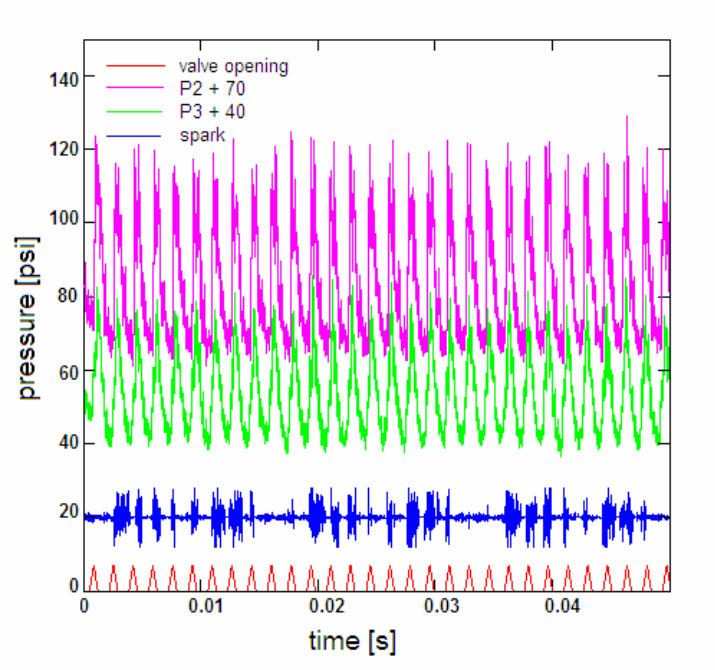

Figure 27: Segment of pressure time history for combustion with 1500 SLPM/air-600 SLPM/H_2.

As discussed in Section 3.3, signal data from the spark was read into the digital oscilloscope so that the role of the spark could be analyzed. The spark, which is fired continuously at 120 Hz during combustion, does not have much effect on the combustion

process beyond igniting combustion at the beginning of the run. Figure 27 is a segment of the pressure time history for combustion with 1500 SLPM/air-600 SLPM/H_2 at an injection frequency of 600 Hz. As shown, detonations still occur at each injection cycle, regardless of constant spark firing at 120 Hz; however, the spark signal does not show clear, distinct pulses with each spark firing.

Figure 28 shows two traces of the spark signal: (a) the spark signal during combustion with 1500 SLPM/air-600 SLPM/H_2 at an injection frequency of 600 Hz shown in Figure 27, and (b) normal spark firing at 120 Hz with only air in the combustion volume. The vertical blue lines in each trace were added to divide the segment into equal parts centered on each spark firing. Each segment is $^1/_{120}$ s in width, except the segments at either end of each plot, which add to form one segment. Although spark firing does not have an effect on the detonation cycle, combustion appears to have an effect on spark firing, as shown in Figure 28(a). A likely explanation for this behavior is that the combustion products have a much lower voltage threshold for arcing than the reactants or regular laboratory air. This lower voltage threshold causes arcing many times in one cycle of the spark generator when combustion products are present, which occurs at peaks in the pressure data. For example, in Figure 27, it appears as though groups of peaks in the spark firing signal occur simultaneously with peaks in pressure data.

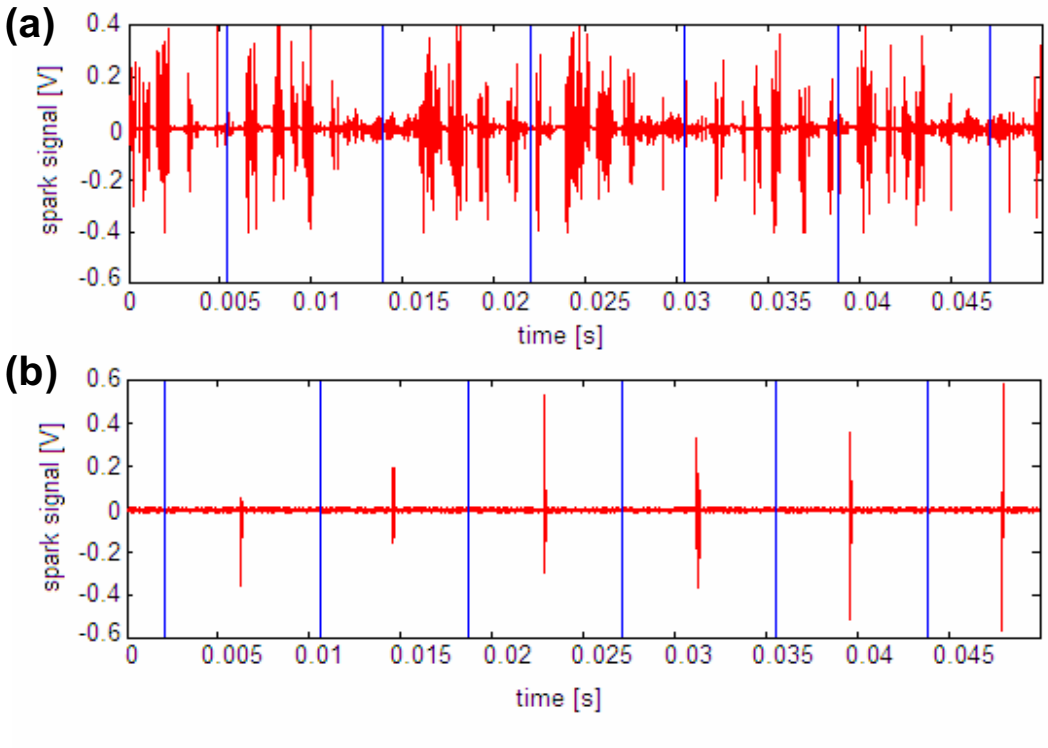

Figure 28: Spark signal: (a) during combustion with 1500 SLPM/air-600 SLPM/H_2; (b) without reactant flows.

If the spark firing is stopped during a run, different behaviors are observed depending on the flow rates and injection frequency. At the lower flow rates (i.e. stoichiometric and O_2-enriched mixtures of air and H_2 with 150, 300, and 450 SLPM/H_2), when spark firing is stopped, the combustion stops. This implies that continuous spark firing is needed to continue combustion. At the higher flow rates (i.e. with 600 and 750 SLPM/H_2) and high

injection frequencies (i.e. >600 Hz), detonations continue after spark firing has stopped in the same manner as with constant spark firing.

Section 4.4 Discussion

Pressure results from the present experiment are similar to those of previous work done by Cutler *et al.* with first generation [15] and second generation [2] models, discussed in Section 1.3. The following discussion will focus mainly on comparison between current model and second generation model, herein referred to as the previous model.

Figure 29 shows results for a non-combusting case: 1500 SLPM/air for the current model, also plotted in Figure 14(b) and (d), and the previous model. In Figure 29(a), RMS pressure at the exit of the combustion volume (P4) is very similar in the two models. RMS pressure in the middle of the combustion volume (P3) is a bit higher in the current model, especially at the lower injection frequencies. RMS pressure at the bottom of the combustion volume (P2) in the current model is nearly twice that of the previous model. The difference in RMS pressure between the two models may be a result of the different cross-sectional shapes of each combustion volume.

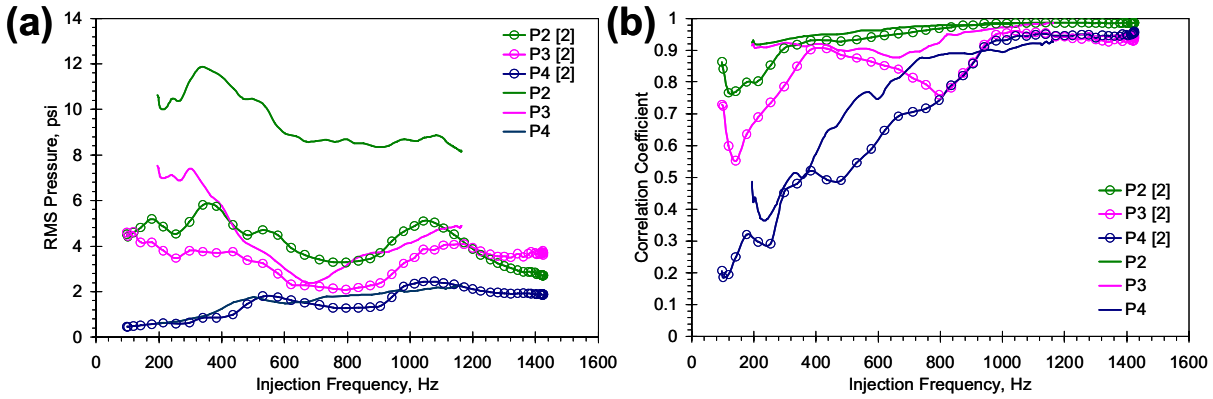

Figure 29: Comparison of results with 1500 SLPM/air to previous work by Cutler *et al.*[2]: RMS pressure plotted in (a), and one-cycle-delay correlation coefficient in (b).

Note that local peaks in RMS pressure occur around the same injection frequencies for both models, ~330 and ~1050 Hz. Figure 29(b) shows one-cycle-delay correlation coefficient as a function of injection frequency for tests with 1500 SLPM/air. It appears as though both models have similar trends in the correlation coefficient, except for P3 in the previous model between 600 and 950 Hz. At high injection frequencies in both models, the correlation coefficient is near one, which indicates periodic waveforms.

Figure 30 plots results for combustion with 1500 SLPM/air-600 SLPM/H_2 for the current model, as plotted in Figure 16(b) and (d), and the previous model. Note that experiments with the current model, unlike previous experiments, did not include injection frequencies past 1000 Hz. This was because it became evident during testing that running the high-speed valve at these injection frequencies past 1200 Hz reduces the lifetime of the bearings.

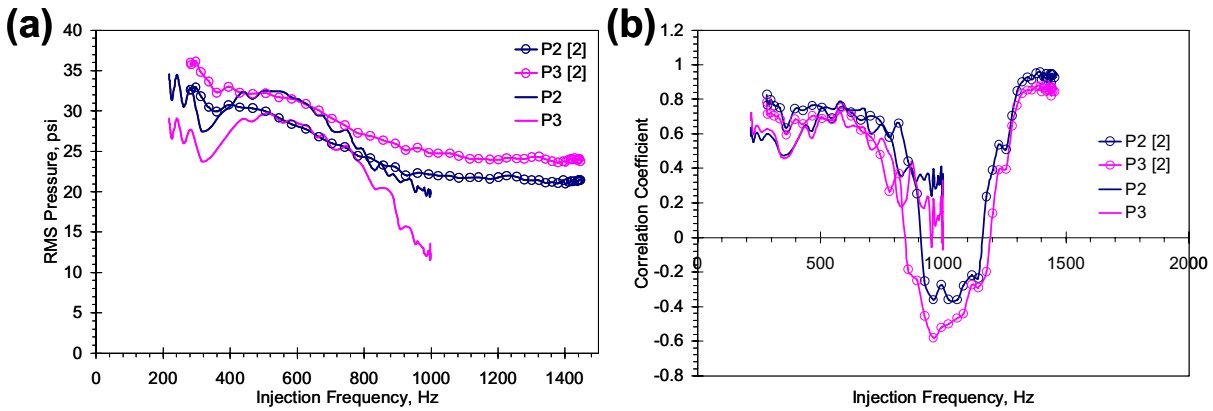

Figure 30: Comparison of results with 1500 SLPM/air-600 SLPM/H_2 to previous work by Cutler *et al.*[2]: RMS pressure plotted in (a), and one-cycle-delay correlation coefficient in (b).

Figure 30(a) shows RMS pressure as a function of injection frequency for pressure gauges located at P2 and P3. In the current model, RMS pressure is greatest at the bottom of the combustion volume (P2), as opposed to the previous model, where RMS pressure is greatest in the middle of the combustion volume (P3), which is directly opposite the location of fuel injection. RMS pressure from the current model, in general, is less than RMS pressure from the previous model, with the exception of P2 RMS pressure between 400 and 800 Hz injection frequency.

Figure 30(b) shows one-cycle-delay correlation coefficient as a function of injection frequency for P2 and P3. The correlation coefficient for the two different models is similar, with the present model having a slightly lower correlation coefficient at injection frequencies less than 500 Hz, and correlation coefficient nearly equal between 500 and 900 Hz. However, around 1000 Hz, there is less correspondence between values of correlation coefficient. In the previous model, the correlation coefficient clearly becomes negative, whereas for the current model, the correlation coefficient is closer to zero, though the data seem rather chaotic. In the previous work, the correlation coefficient rises to ~1 around 1400 Hz indicating periodic combustion at each injection cycle. It is suspected that if experiments were conducted at these higher injection frequencies (up to 1500 Hz), the current model would exhibit the same sort of behavior, as plotted in Figure 30(b).

The main contribution of the present work is the measurement of thrust and I_{sp}. Table 2 summarizes the results of thrust balance tests presented in Section 4.2. Maximum thrust and I_{sp} are tabulated for each reactant flow rate along with corresponding injection frequency at which the maximum occurs. The last column in Table 2 is the percent difference in I_{sp} for each case, using the 1500 SLPM/air-600 SLPM/H_2 case at ~600 Hz as the reference value. This result was chosen to be the reference I_{sp} because it was the case with a stoichiometric reactant mixture which produced the best results.

The low I_{sp} value at the two lowest reactant flow rates, 375 SLPM/air-150 SLPM/H_2 and 750 SLPM/air-300 SLPM/H_2, yield a large percent difference to the reference case. This is attributed to incomplete combustion at these low flow rates. At the higher stoichiometric flow rates, 1125 SLPM/air-450 SLPM/H_2 and 1875 SLPM/air-750 SLPM/H_2, the percent difference is much smaller, -5.82 % and -3.10%, respectively. Considering the two fuel-lean cases, maximum I_{sp} at 1875 SLPM/air-650 SLPM/H_2 had only a -0.65% difference from the

reference case, whereas maximum I_{sp} at 1875 SLPM/air-600 SLPM/H_2 had a larger difference of 14.47%.

Flow rate of Air, SLPM	**Flow rate of H_2, SLPM**	**Injection Frequency, Hz**	**Thrust, lb**	**I_{sp}, s**	**difference in I_{sp}, %**
375	150	750	0.391	789	-69.79%
750	300	750	1.806	1822	-30.25%
1125	450	600	3.656	2460	-5.82%
1500	**600**	**600**	**5.176**	**2612**	--
1875	750	525	6.269	2531	-3.10%
1875	600	425	5.926	2990	14.47%
1875	650	300	5.572	2595	-0.65%

Table 2: Summary of performance at 600 Hz injection frequency with various reactant flow rates.

Two possibilities may explain why peak thrust and I_{sp} do not occur at the expected resonant frequency of 600 Hz in the fuel-lean cases. One possibility is that the resonant frequency has shifted from 600 Hz to a lower value; however, this trend would be difficult to explain and there is no evidence to that effect in the plots of RMS pressure and correlation coefficient. As discussed in Section 4.1, Figure 20(a) has local peaks in RMS pressure for all three conditions at ~600 Hz. Another possibility is that the fuel-lean cases tend toward a high I_{sp}, but dilution by air causes incomplete combustion at high injection frequencies. If this is the case, a larger I_{sp} may be achieved by replacing some of the air flow with O_2. The results suggest the fuel-lean cases may have the potential to outperform the stoichiometric cases, if steps were taken to ensure complete combustion.

Reference	Frequency, Hz	Volume V in^3	Fill Fraction	Thrust T lb	Isp, s	T/V, lb/in^3
Nicholls[5]	26.7	226	<1	3.2	2100	0.0141
AFRL (a) [13]	16	452	1	6.7	3750	0.0147
AFRL (b) [13]	16	452	0.3	3.7	7100	0.0083
GE-GRC[11]	10	485	1	12.9	1074	0.0266
Zhang[12]	32	2372	N/A	--	~2000	--
Present Work	600	3	1.71*	5.18	2611	1.73

Table 3: Summary of results for various experiments.

* Fill fraction for assumed combustion tube pressure of 1 atm.

It is useful to compare the thrust balance and I_{sp} results from this experiment to those of H_2-fueled PDEs from other research facilities. Table 3 lists the results from such experiments, as discussed in Section 1.2. Unless otherwise stated in the published works, thrust values listed in Table 3 are assumed to be total thrust measured for each experiment. For Ref. [11], the thrust measurement taken is the maximum value published, which is the

value uncorrected for the effect of "hot jet thrust". Although the actuator discussed here did not produce the largest specific impulse compared to similar work, it has larger I_{sp} than those of many of the references. Also, the actuator is much smaller than for the comparable PDEs. Figure 31 is a plot of thrust per unit combustion tube volume versus injection frequency for the various experiments listed in Table 3.

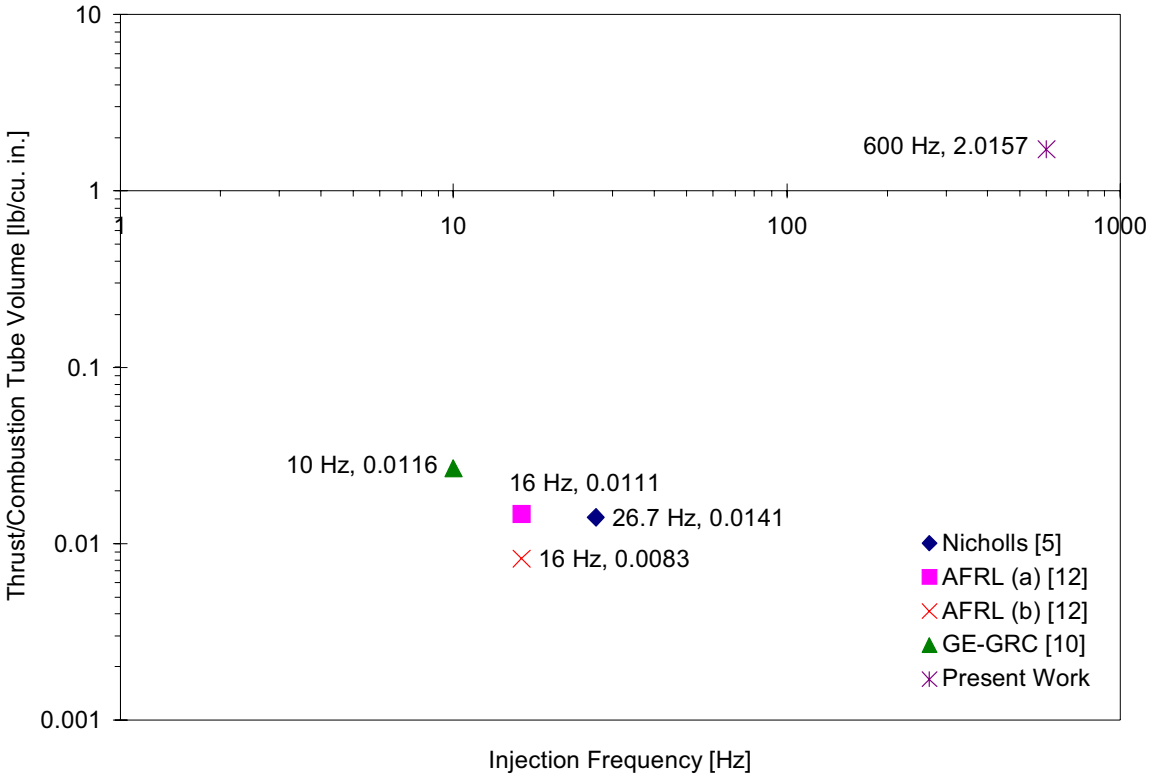

Figure 31: Maximum thrust per unit volume plotted against injection frequency for various experiments.

For the results shown in Table 3 for the present experiment, combustion tube fill fraction is reported as 1.71 for 1500 SLPM/air-600 SLPM/ H_2 at 600 Hz injection frequency. This value is based on the assumption that the combustion tube pressure is 1 atm (~14.7 psia), and implies that some of the reactants are "spilling" out of the tube during operation. As discussed previously, in Section 4.1, the combustion tube pressure oscillates such that just prior to detonation (i.e., just after injection of the reactants) the pressure is higher than 14.7 psia. Given that the pressure within the tube is higher than atmospheric, it is likely that the reactants do not in fact significantly spill from the tube.

Consider the experiment listed in Table 3 that produced the highest I_{sp}, which was developed by the Air Force Research Laboratories [13]. Results reported were for a single aluminum tube (2.0" ID x 36") with a stoichiometric mixture of pre-mixed air and hydrogen and a 50% clean air purge fill ratio [13]. Figure 32 is a plot of the results taken from the AFRL paper which shows thrust and I_{sp} as a function of fill fraction for PDE operation at 12 Hz and 16 Hz. Note that thrust data plotted for 16 Hz have been scaled to match with data from 12 Hz. Figure 32 shows that maximum thrust occurs with a fill fraction of at least unity, corresponding to an I_{sp} of approximately 3750 s.

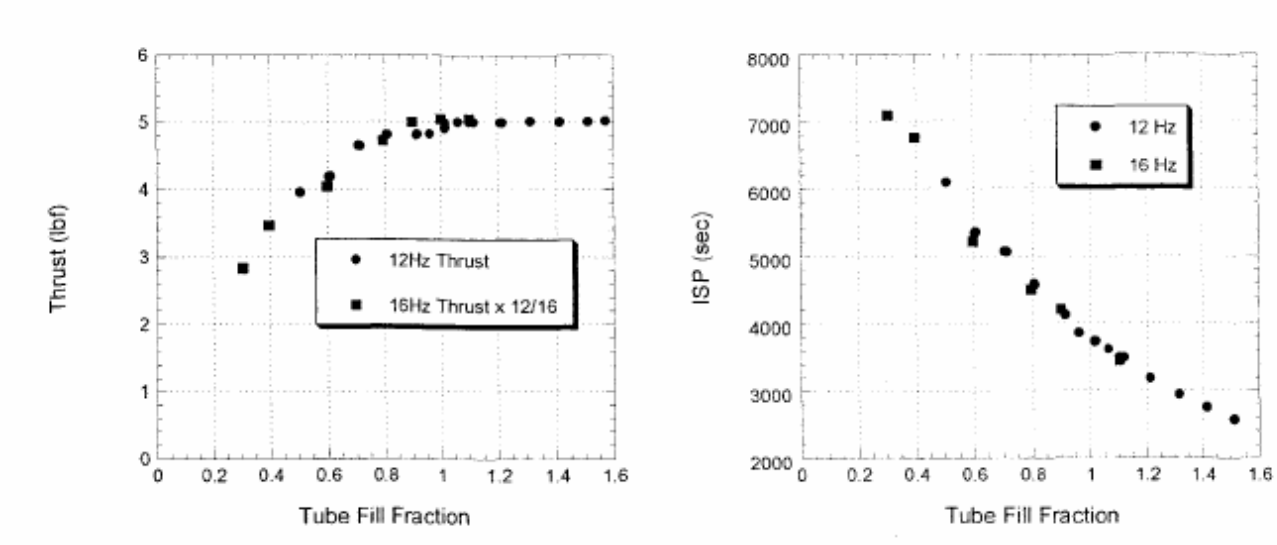

Figure 32: Thrust (left) and fuel specific impulse (right) versus tube fill fraction, Schauer *et al* [13].

Figure 32 also shows that I_{sp} is greatest with fill fraction less than unity, and decreases as fill fraction is increased; however, low fill-fraction does not yield very high thrust. When fill fraction is less than unity, only part of the combustion tube is filled with fresh reactants while the remainder of the tube contains air (from the purge cycle) or hot-expanded products from the previous cycle. It may be that a similar result would be obtained by running the model fuel-lean, as was done in the present experiment. Results from fuel-lean tests conducted in the present experiment are inconclusive, since I_{sp} only increased a small amount, and only at lower than resonant frequencies. This effect may have been offset by other adverse effects of diluting the reactants, such as reduction in the reactivity of the reactants.

This result, which shows that lower fill fraction (or perhaps fuel-lean conditions) will yield higher I_{sp}, is probably analogous to the effect of increasing bypass ratio in turbofan engines – more mass flow is processed through the engine for a given flow of fuel. In turbofan engines, higher bypass ratios correlate with better specific fuel consumption and better propulsive efficiency.

Consider the experiment listed in Table 3 that produced the lowest I_{sp}, which was developed by a team at the GE Global Research Center [11]. Again, this value for I_{sp} was not explicitly stated in the reference paper, but was calculated using the maximum thrust and mass flow rates reported in the paper. The author is unsure why this device fared so poorly compared to the PDE developed by AFRL, especially since they are similar in size and thrust measured. It is possible that the method of calculation was flawed, or the figures used were incorrect, which would yield an incorrect I_{sp}.

Results reported by Zhang *et al.* include data from single-shot detonation experiments as well as operation of the PDE at injection frequencies of up to 32 Hz [12]. Maximum I_{sp} reported was 2380 s, which corresponds with a single-shot detonation experiment. For operation at 32 Hz, I_{sp} is reported to be ~2000 s, but thrust measurement data were not stated in the paper. Information given in the paper was insufficient to calculate the thrust generated by this device.

Figure 31 clearly shows the advantages of the current device over other PDEs. When normalized by combustion tube volume, the actuator presented here is far superior to the PDEs considered. The compact size of the actuator results in a low weight-to-thrust ratio, which is desirable in aircraft and missile propulsion systems. It is also important to note that the actuator presented here operated at much higher injection frequencies than those in the other experiments listed.

The ability for high-frequency operation of the device presented here, in addition to its compact size, make it worthy for continued research in various applications. One possible application of this device is high-speed flow control. The high specific impulse generated and the high frequencies of operation that can be attained make this device desirable for boundary layer separation control at high speeds, specifically separation control in hypersonic engine inlets.

The pulsed detonation actuator presented here poses an attractive alternative to jet turbine engines for small disposable engines because of its potentially low weight and high performance. While it may not rival the performance of a large jet engine, its compact size may be useful in small-scale propulsion applications, including high-speed munitions, small missiles, supersonic reconnaissance vehicles, and launch vehicles for mini-satellites [6]. Its size may also make it desirable for use as a pressure rise combustor in gas turbine engines. Previous work has shown that the use of PDEs at various positions within a gas turbine engine can increase the efficiency and overall performance of the engine [1].

Chapter 5 - Summary and Conclusions

Experiments have been conducted to investigate a pulsed detonation actuator. The combustion volume was 8" in length and had a rectangular cross-section of 0.5" x 0.75". A stoichiometric mixture of H_2 and air was supplied to the actuator at various flow rates and at frequencies of up to 1000 Hz. Thrust balance measurements were conducted to determine the thrust and I_{sp} generated by the model at different operating conditions.

The major contribution of the present work, as opposed to previous work [2], is that a thrust balance system was developed and used in order to determine the thrust generated during operation. As expected, detonations in a stoichiometric mixture of H_2/air were accomplished in the short $\lambda/4$ resonant tube, specifically at high reactant flow rates at the resonant frequency (~600 Hz) and half the resonant frequency (~285 Hz). Addition of O_2 into the reactant mixture helped enhance combustion at lower reactant flow rates. At higher flow rates, mixing and combustion of H_2 and air was already complete; therefore, the addition of O_2 did not change the behavior of the actuator.

Maximum thrust attained was ~6.0 lb_f at the highest reactant flow rate of 1875 SLPM/air-750 SLPM/H_2 at the resonant frequency, ~600 Hz. As expected, thrust increased with reactant flow rate. Specific impulse was consistent for the three highest reactant flow rates at the resonant frequency, with less than a 6% difference from the reference value of 2611 s at 1500 SLPM/air-600 SLPM/H_2. At the lower flow rates, detonations did not occur at each injection cycle and combustion was not complete, causing low thrust and I_{sp}.

Fuel-lean conditions were also tested to determine the effect on thrust. Two fuel-lean cases were tested to compare to a case with a stoichiometric mixture of 1875 SLPM/air-750 SLPM/H_2. Detonations continued to occur at the resonant frequency of ~600 Hz; however, this injection frequency did not yield maximum thrust or I_{sp}, as it did in the stoichiometric cases. Thrust generated at the fuel-lean conditions ranged between 4.5 and 6.0 lb. A maximum I_{sp} of 2990 s was calculated for a reactant mixture of 1875 SLPM/air-600 SLPM/H_2 at an injection frequency of ~425 Hz. It is speculated that there are two offsetting trends whose relative importance depends on frequency. First, incomplete reaction in the fuel-lean cases would be expected to decrease I_{sp}. However, fuel-lean conditions are similar to reducing the combustion tube fill fraction, which has been shown to increase I_{sp}. Further studies will need to be conducted in order to clearly understand the effects of operating with fuel-lean conditions.

One difference in the current device from the previous model is the rectangular cross-section, which enables the model to be fitted with windows. Internal flow visualization of the combustion volume was not conducted in the present work, but images of the combustion volume during detonation cycles will lead to a better understanding of the gas dynamics occurring within the device. In future work, flow visualization of the combustion volume and exhaust jet should be conducted. Also, higher frequencies of operation, up to 1400 Hz, should be tested to observe the behavior of the device at higher injection frequencies. As in past models [2][15], operation at around 1400 Hz, which corresponds to the $3\lambda/4$ waveform, resulted in perfectly periodic deflagration combustion at each injection cycle. This behavior may also be observed in the current model if further tests were conducted.

This device was developed primarily for flow control applications. The high specific

impulse and high frequencies of operation attained with this device give it much promise in high-speed boundary layer separation control applications, especially hypersonic engine inlets. However, possible applications are not limited to flow control. Other applications include small-scale propulsion applications—such as high-speed munitions, small missiles, supersonic reconnaissance vehicles, and launch vehicles for mini-satellites, and pressure-rise combustors for gas turbine engines. Because of its great potential as a small-scale propulsion device, future research with this device is encouraged.

References

[1] Rasheed, A., Furman, A., and Dean, A.J. "Wave Interactions in a Multi-tube Pulsed Detonation Combustor-Turbine Hybrid System." AIAA-2006-4447, *AIAA/ASME/SAE/ASEE Joint Propulsion Conference and Exhibit*, Sacramento, CA, 9-12 July 2006.

[2] Cutler, A.D., and Drummond, J.P. "Toward a High-Frequency Pulsed Detonation Actuator." AIAA 2006-555, *44th AIAA Aerospace Sciences Meeting and Exhibit*, Reno, NV, 9-12 January 2006.

[3] Ma, F., Choi, J.Y., and Yang, V. "Thrust Chamber Dynamics and Propulsive Performance of Single Tube Pulse Detonation Engines." *Journal of Propulsion and Power*, Vol.12, No. 3, May – June 2005.

[4] Eidelman, S., and Grossman, W. "Pulsed Detonation Engine Experimental and Theoretical Review." AIAA 92-3168, *AIAA/ASME/SAE/ASEE 28th Joint Propulsion Conference and Exhibit*, Nashville, TN, 6-8 July 1992.

[5] Nicholls, J.A., Wilkinson, H.R., and Morrison, R.B. "Intermittent Detonation as a Thrust Producing Mechanism." *Jet Propulsion*, Vol. 27, pp. 534-541, 1957.

[6] McManus, K., Furlong, E., Leyva, I., and Sanderson, S. "MEMS-Based Pulse Detonation Engine for Small-Scale Propulsion Applications." AIAA 2001-3469, *27th AIAA/ASME/SAE/ASEE Joint Propulsion Conference and Exhibit*, Salt Lake City, UT, 8-11 July 2001.

[7] Crittendon, T, and Glezer, A. "Combustion-Driven Jet Actuators for Flow Control." AIAA-2001-2768, *31st AIAA Fluid Dynamics Conference and Exhibit*, Anaheim, CA, 11-14 June 2001.

[8] Werrell, K.P. *The Evolution of the Cruise Missile,* AD-A162 646. September 1985, pp. 41-43.

[9] Kailasanath, K. "Review of Propulsion Applications of Detonation Waves." *AIAA Journal*, Vol. 38, No. 9, September 2000.

[10] Litke, P.J., Schauer, F.R., Paxson, D.E., Bradley, R.P, and Hoke, J.L. "Assessment of the Performance of a Pulsejet and Comparison with a Pulsed-Detonation Engine." AIAA-2005-228, *43rd AIAA Aerospace Sciences Meeting and Exhibit*, Reno, NV, 10-13 January 2005.

[11] Rasheed, A., Tangirala, V.E., Pinard, P.F., and Dean, A.J. "Experimental and Numerical Investigations of Ejectors for PDE Applications." AIAA-2003-4971, *39th AIAA/ASME/SAE/ASEE Joint Propulsion Conference and Exhibit*, Huntsville, AL, 21-23 July, 2003.

[12] Zhang, F.Y., Fujiwara, T., Miyasaka, T., Nakayama, E., and Hattori, T. "Detonation Studies of High-Frequency-Operation Pulse Detonation Engine with Air/Hydrogen." AIAA-2003-1169, *41st Aerospace Sciences Meeting and Exhibit*, Reno, NV, 6-9 January, 2003.

[13] Schauer, F., Stutrud, J., and Bradley, R. "Detonation Initiation Studies and Performance

Results for Pulsed Detonation Engine Applications." AIAA 2001-1129, *39th AIAA Aerospace Sciences Meeting and Exhibit*, Reno, NV, 8-11 January, 2001.

[14] Heiser, W.H., and Pratt, D.T. "Thermodynamic Cycle Analysis of Pulse Detonation Engines." *AIAA Journal of Propulsion and Power*, Vol. 18, No. 1, January – February 2002.

[15] Cutler, A.D., Beck, B.T., Wilkes, J.A., Drummond, J.P., Alderfer, D.W., and Danehy, P.N. "Development of a Pulsed Combustion Actuator for High-Speed Flow Control." AIAA-2005-1084, *43rd AIAA Aerospace Sciences Meeting and Exhibit*, Reno, NV, 10-13 January 2005.

REPORT DOCUMENTATION PAGE

Form Approved
OMB No. 0704-0188

1. REPORT DATE *(DD-MM-YYYY)*	2. REPORT TYPE	3. DATES COVERED *(From - To)*
01-06-2008	Contractor Report	

4. TITLE AND SUBTITLE

Pressure and Thrust Measurements of a High-Frequency Pulsed-Detonation Actuator

5a. CONTRACT NUMBER

5b. GRANT NUMBER

5c. PROGRAM ELEMENT NUMBER

6. AUTHOR(S)

Nguyen, Namtran C.; and Cutler, Andrew D.

5d. PROJECT NUMBER

NNL06AA16A

5e. TASK NUMBER

5f. WORK UNIT NUMBER

526282.01.07.04.06

7. PERFORMING ORGANIZATION NAME(S) AND ADDRESS(ES)

NASA Langley Research Center
Hampton, VA 23681-2199

The George Washington University
1 Old Oyster Point Road
Newport News, VA 23602

8. PERFORMING ORGANIZATION REPORT NUMBER

9. SPONSORING/MONITORING AGENCY NAME(S) AND ADDRESS(ES)

National Aeronautics and Space Administration
Washington, DC 20546-0001

10. SPONSORING/MONITOR'S ACRONYM(S)

11. SPONSORING/MONITORING REPORT NUMBER

NASA/CR-2008-215315

12. DISTRIBUTION/AVAILABILITY STATEMENT

Unclassified - Unlimited
Subject Category 34 Availability: NASA CASI (301) 621-0390

13. SUPPLEMENTARY NOTES

Langley Technical Monitor: Aaron H. Auslender An electronic version can be found at http://ntrs.nasa.gov

14. ABSTRACT

This paper describes the development of a small-scale, high-frequency pulsed detonation actuator. The device utilized a fuel mixture of H2 and air, which was injected into the device at frequencies of up to 1200 Hz. Pulsed detonations were demonstrated in an 8-inch long combustion volume, at ~600 Hz, for the λ/4 mode. The primary objective of this experiment was to measure the generated thrust. A mean value of thrust was measured up to 6.0 lb, corresponding to specific impulse of 2611 s. This value is comparable to other H2-fueled pulsed detonation engines (PDEs) experiments. The injection and detonation frequency for this new experimental case was ~600 Hz, and was much higher than typical PDEs, where frequencies are usually less than 100 Hz. The compact size of the model and high frequency of detonation yields a thrust-per-unit-volume of approximately 2.0 lb/in3, and compares favorably with other experiments, which typically have thrust-per-unit-volume values of approximately 0.01 lb/in3.

15. SUBJECT TERMS

Combustion; Detonation; Experiments; Pulse detonation engines; Pulsejets

16. SECURITY CLASSIFICATION OF:			17. LIMITATION OF ABSTRACT	18. NUMBER OF PAGES	19a. NAME OF RESPONSIBLE PERSON
a. REPORT	b. ABSTRACT	c. THIS PAGE			STI Help Desk (email: help@sti.nasa.gov)
U	U	U	UU	58	19b. TELEPHONE NUMBER *(Include area code)* (301) 621-0390